minerals

MDPI

Article

Microscopic-Scale Examination of the Black and Orange–Yellow Colours of Architectural Glazes from Aššur, Khorsabad and Babylon in Ancient Mesopotamia

Fanny Alloteau [1,*], Odile Majérus [2], Floriane Gerony [2], Anne Bouquillon [3], Christel Doublet [3], Helen Gries [4], Anja Fügert [5], Ariane Thomas [6] and Gilles Wallez [2]

1 Rathgen-Forschungslabor, Staatliche Museen zu Berlin, Stiftung Preußischer Kulturbesitz, 14059 Berlin, Germany
2 Chimie ParisTech, Centre National de la Recherche Scientifique (CNRS), Institut de Recherche de Chimie Paris (IRCP), PSL University, 75005 Paris, France; odile.majerus@chimieparistech.psl.eu (O.M.); floriane.gerony@chimieparistech.psl.eu (F.G.); gilles.wallez@chimieparistech.psl.eu (G.W.)
3 Centre de Recherche et de Restauration des Musées de France (C2RMF), Palais du Louvre, 75001 Paris, France; anne.bouquillon@culture.gouv.fr (A.B.); christel.doublet@culture.gouv.fr (C.D.)
4 Vorderasiatisches Museum, Staatliche Museen zu Berlin, Stiftung Preußischer Kulturbesitz, 10178 Berlin, Germany; h.gries@smb.spk-berlin.de
5 Orient Department, German Archaeological Institute, 14195 Berlin, Germany; anja.fuegert@dainst.de
6 Département des Antiquités Orientales, Musée du Louvre, 75001 Paris, France; ariane.thomas@louvre.fr
* Correspondence: f.alloteau@smb.spk-berlin.de

check for updates

Citation: Alloteau, F.; Majérus, O.; Gerony, F.; Bouquillon, A.; Doublet, C.; Gries, H.; Fügert, A.; Thomas, A.; Wallez, G. Microscopic-Scale Examination of the Black and Orange–Yellow Colours of Architectural Glazes from Aššur, Khorsabad and Babylon in Ancient Mesopotamia. *Minerals* **2022**, *12*, 311. https://doi.org/10.3390/min12030311

Academic Editors: Marco Benvenuti and Adrián Durán Benito

Received: 23 January 2022
Accepted: 23 February 2022
Published: 28 February 2022

Publisher's Note: MDPI stays neutral with regard to jurisdictional claims in published maps and institutional affiliations.

Copyright: © 2022 by the authors. Licensee MDPI, Basel, Switzerland. This article is an open access article distributed under the terms and conditions of the Creative Commons Attribution (CC BY) license (https://creativecommons.org/licenses/by/4.0/).

Abstract: Three major corpora of architectural glazed bricks from Ancient Mesopotamia dating to the Neo-Assyrian (Aššur and Khorsabad sites) and the Neo-Babylonian (Babylon site) Periods have been submitted to an in-depth comparative study of the orange–yellow and black glazes. Distinct hues in the orange–yellow range were observed according to the archaeological site. They appear to have been well mastered by the glassmakers, consisting in the ex situ preparation of the antique lead antimonate pigment and its mixing with transparent soda-lime glass frit or with the glass-forming components. The intentional addition of hematite or of Cu^{2+} colouring ions in a controlled amount is suggested in two cases. SEM-EDX and Raman analysis of the lead antimonate pigments have pointed out different chemical substitutions in their pyrochlore structure, mainly Fe^{3+} in the Sb^{5+} site and Ca^{2+} in the Pb^{2+} site, the proportion of which being correlated to the pigment shade (from pale yellow to orange–red). Part of these substitutions arises from the chemical reaction of the pigment with the hematite and glass melt during firing. Regarding the black glazes, an unexpected colouring technique involving copper sulphide nanoparticles together with the chromophore Fe^{3+}-S^{2-} is highlighted for Khorsabad (8th century BC) and for Babylon (6th century BC). For Aššur blacks, the study reveals a change in their colouring technique between the 9th and 8th centuries BC, from a colouration with Mn oxides to an enigmatic one that could also have involved copper sulphide nanoparticles.

Keywords: coloured glazes; black glazes; yellow glazes; orange glaze; glass; colour; Mesopotamia; lead antimonate; copper sulphide nanoparticles; chromophore Fe^{3+}-S^{2-}

1. Introduction

For nearly a millennium, between the 14th and the 4th century BC, monumental glazed decorations adorned architectural facades of major cities in Elam (south-west of present-day Iran) and in ancient Mesopotamia (present-day Iraq for its most part) [1]. First attested in Elam in the second half of the 2nd millennium BC, these large coloured decorations then became part of the visual universe of Mesopotamia from the 9th century BC to the 6th century BC under the two successive empires, Neo-Assyrian (900–610 BC) and Neo-Babylonian (626–539 BC), and would have lasted until the Persian Achaemenid Empire (539–330 BC) in Persepolis, Susa and again in Babylon. The Ishtar Gate of the city of

Babylon for instance, reconstituted in the Vorderasiatisches Museum (VAM) in Berlin, or the frieze of the Archers of the city of Susa, preserved in the musée du Louvre in Paris, allow us to appreciate nowadays the monumentality of such constructions. These decorations are the mark of a flourishing technological development of glazing on bricks that took place in these pioneer regions of the Ancient Near East from the 14th century BC onwards, shortly after the appearance of the first core formed glass vessels [1–4]. Thus, it appears that the development of this glazing technology had a profound impact on both the material and sensory culture of these ancient civilizations. In order to improve our knowledge and to preserve and transmit this history, the physico-chemical study of these glazed decorations is of major interest. This indeed contributes to helping museums reconstitute these decors in an approach of cultural and sensory knowledge and to investigate these technical innovations and the transfer of know-how in these regions, including the connection with metallurgy and glass production techniques. However, one major issue for a broad and detailed investigation of these glazed artefacts is the poor state of preservation of most of them. Heavy weathering is indeed reported for numerous glazed clay ceramics dated back to the end of the Bronze Age or to the Iron Age and excavated at various sites in Iran and in Iraq [5–12], as a consequence, in particular, of the environmental ground deposit conditions particularly damp and saline in these regions [13]. Note that the so-called "weathering" of glass refers to its degradation by chemical reaction of the glassy surface with groundwater during burial.

Numerous scientific studies of these early glazed materials carried out so far have focused on the existing glaze colours and their colouring agents [14]. From archaeological evidence, it seems that the glazing industry remarkably evolved during the Neo-Assyrian Period for greater polychromy of the glazed decorations. It was during the later Neo-Babylonian period that dark blue glazes coloured with cobalt oxide would have appeared as architectural ornaments. The main group of glaze colours referenced in the literature for these periods and through until the Achaemenid Period are white, orange–yellow, blue–greenish, and black.

The VAM and the musée du Louvre's département des Antiquités orientales each have a major corpus of Neo-Assyrian glazed bricks in their collections. Within the VAM, it is the corpus of Aššur (north of present-day Iraq—Figure 1) with more than 3000 glazed bricks of which the major part is identified as remains of the temple of the god Aššur, the main sanctuary of Assyria (9th–7th century BC covering the reign of Sargon II in the late 8th century BC), and a lesser part as remains of the temple of Anu Adad and the city walls (both early 9th century BC). Since 2016, a reconstruction work of the glazed facades of the temple of the god Aššur has taken shape in the VAM through the "GlAssur" Project ("The Reconstruction of the Glazed Brick Façades from Ashur in the Vorderasiatisches Museum Berlin") [15–17]. Within the musée du Louvre, it is the corpus of Khorsabad (north of present-day Iraq—Figure 1) with 58 glazed bricks belonging to the Royal Palace dating from the foundation of Dûr-Sharrukin during the reign of Sargon II (721–705 BC), that have been thoroughly described in Refs. [18,19]. In parallel with these recent contextualization works, a micro-scale examination of the glazes of these bricks has been conducted. For comparison purposes, this research has also encompassed a detailed study of some Neo-Babylonian coloured glazes belonging to the famous and remarkably well preserved architectural decoration of Babylon (south of present-day Baghdad in Iraq—Figure 1) [20], stored in the VAM collection.



Figure 1. Location of Aššur, Khorsabad and Babylon and of some other archaeological sites in ancient Mesopotamia (present day Iraq for its most part) and in Elam (south-west of present-day Iran) with evidence of early glaze production. © d-maps.com, accessed on 13 February 2022.

For each of these three corpora, the colour palette of the glazes consists of the white, turquoise–green–blue, orange–yellow, and black shades, which are widely reported colours for glassy artefacts belonging to the considered period and region [14,21]. The detail of the colour palette and the related colouring agents per corpus is given in the Supplementary Materials (Table S1). In this article, we focus on the orange–yellow and black glazes from Aššur, Babylon, and Khorsabad. The main colouring agents of these orange–yellow glazes are lead antimonates that play both the role of opacifier and pigment, as expected for glassy materials from the Ancient Near East [21,22]. Lead antimonates-based pigments were widespread in Antiquity from Egypt to Rome, then were more scarce during the Middle Ages, before being reused on a large scale in Renaissance Italy under the name of "Naples yellow" [23–26]. The chemical diversity of these antimonates, thanks to the numerous substitutions permitted by their pyrochlore structure and their good state of conservation, certainly make them sensitive "markers" of the chemical, thermal and kinetic conditions in the glazing mixture, likely to provide a wealth of information on the manufacturing processes. In addition to studying ancient pigments, researchers have approached these pigments by synthesizing them in a laboratory in order to better understand the conditions of their formation, their variability, and stability within glazes [7,24,27–29]. In the present study, various shades of lead antimonate pigments in the orange–yellow range are observed for Aššur, Khorsabad, and Babylon. To the purpose of a detailed comparison between the three corpora and a better understanding of the origin of the colours, an in-depth characterization of these pigments has been undertaken by means of Optical Microscopy, Scanning Electron Microscopy coupled with Energy Dispersive X-ray Spectroscopy (SEM-EDX), and μ-Raman Spectroscopy. Fe-substituted lead antimonates have been synthesized as references to help the interpretation of the Raman spectra.

These analytical methods were also used to draw hypotheses about the origin of the black colour of the Aššur, Khorsabad, and Babylon glazes. The literature for the antique black glazes is sparse. The main colouring agents explaining the dark colours of most glazes and glasses and the various shades between brown, reddish-brown, and black are

the manganese and/or iron oxides [5,8,30,31]. The literature also mentions the use of copper in addition to iron-bearing materials [6,11,32] or of more or less high contents of cobalt oxide that can be added to enhance the darkness [22]. Moreover, it is known that low Fe contents are sufficient to colour glass in amber/green/black when present in the form of the chromophore Fe^{3+}-S^{2-}. This chromophore was used in ancient times to colour glass vessels, for instance [33,34]. Nevertheless, the black glazes of the present study are related to an unexpected and little-known technique, implying copper sulphide nanoparticles, with a possible contribution of the Fe^{3+}-S^{2-} chromophore in the glass matrix that will be discussed.

In order to shorten and lighten the text, the three corpora of bricks are referred to as Khorsabad bricks, Aššur bricks, Babylon bricks in this article.

2. Materials and Methods

Aššur and Babylon bricks were studied at the Rathgen-Forschungslabor in Berlin, and Khorsabad bricks were studied at the Centre de Restauration et de Recherche des Musées de France (C2RMF) in Paris.

2.1. Short Description of the Studied Bricks

For this study, a few glazed bricks or glazed brick fragments displaying an orange–yellow and/or a black glaze were selected in the whole corpus stored in the museum collections of the musée du Louvre (Neo-Assyrian bricks from Khorsabad—8th century BC) and of the VAM in Berlin (Neo-Assyrian bricks from Aššur—9th–7th century BC, and Neo-Babylonian bricks from Babylon—6th century BC). The photographs and the name of the studied glazed bricks or glazed brick fragments are given in Figure 2 (Khorsabad), Figure 3 (Aššur), and Figure 4 (Babylon). This selection was based on their conservation state and, for the corpus of Aššur, on their representativeness of different production times (9th century BC or 8th–7th century BC). This dating for Aššur was carried out in the framework of the GlAssur Project, based on the study of the iconography, the inscriptions, the find contexts, and other physical characteristics, such as their dimensions, fitter's marks, stamps, or impressions [15]. All three corpora show evident clues of alteration, but their intensity levels differ from one corpus to another. Aššur bricks are in the poorest state of conservation, although those selected for the study from among the 3000 bricks kept at the VAM are the best preserved. Nevertheless, their glazes, when still present, appear heavily weathered with faded colours to the naked eyes. Noticeably, extreme cases of decolouration are encountered for the black glazes, which display nearly always whitish areas (see, for instance, the black contour lines of brick A-810791 in Figure 3).

On the contrary, the glazes from Babylon appear remarkably well preserved, with some signs of weathering that remain localized on the glaze surface or more in-depth but limited to the surrounding of fine cracks as revealed by SEM observations of cross-sections. The glazes on Khorsabad bricks are intermediate with important variations of the alteration state between the bricks, but systematically it was possible to study orange–yellow and black areas with the almost unaltered surface.

2.2. Sampling and Preparation of Cross-Sections

Millimetric samples were taken from the glazed bricks or from the fragments of glazed bricks using a scalpel. They were carefully embedded in epoxy resin, then cut with a diamond saw and polished with Micro-Mesh abrasive sheets up to 1200 grain (Aššur, Babylon) or with diamond pastes up to ¼ µm (Khorsabad) to obtain polished cross-sections through the glazes and into the clay bodies.

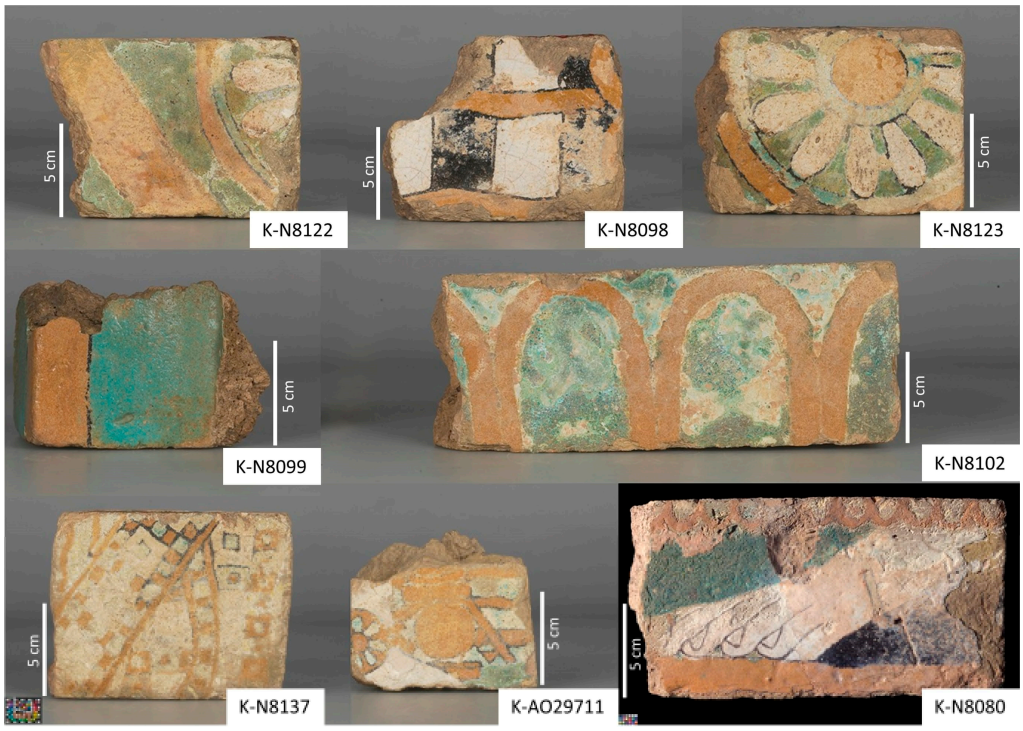


Figure 2. Colour-calibrated photographs of the glazed bricks from Khorsabad selected for this study. © Anne Maigret, C2RMF. All these bricks are dated from the foundation of Dûr-Sharrukin on the site of Khorsabad during the reign of Sargon II (721–705 BC). Two other bricks not shown in this figure have also been studied: K-N8105 (similar to K-N8102) and K-AO29710 (representing a flower).

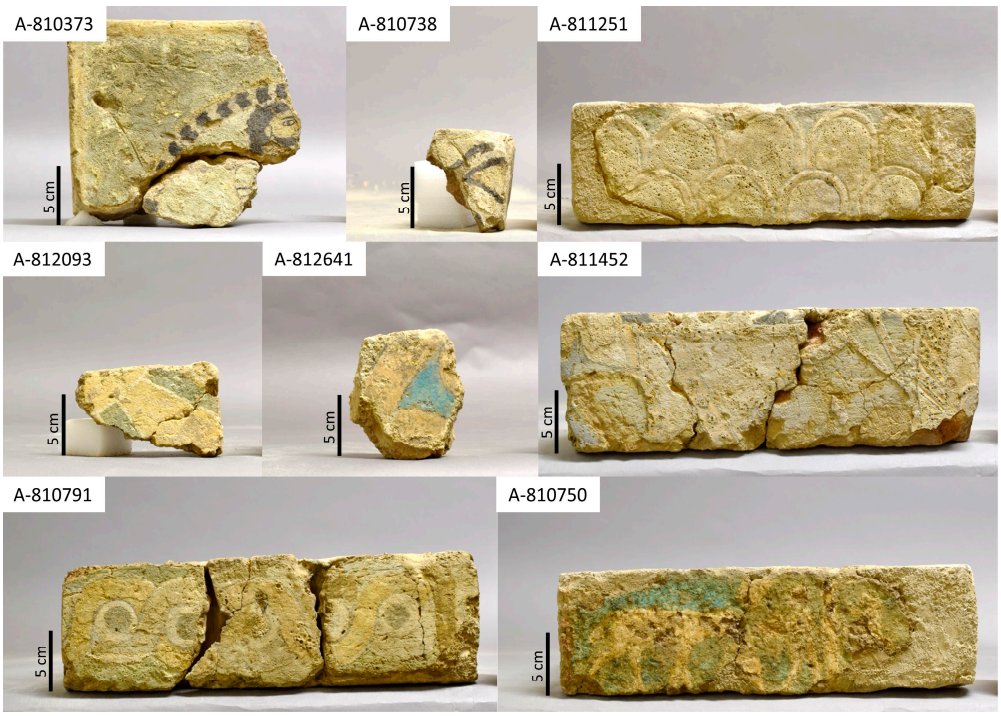


Figure 3. Photographs of the glazed bricks/glazed brick fragments from Aššur selected for this study. The brick fragment A-810373 is dated from the 9th century BC, the brick fragment A-810738 is assumed to date from the 9th century BC, the other bricks are dated or are assumed to date from the 8th–7th century BC (temple of the god Aššur), except the brick A-810791 that remains undated. © Vorderasiatisches Museum, SMB, photo: GlAssur Project.

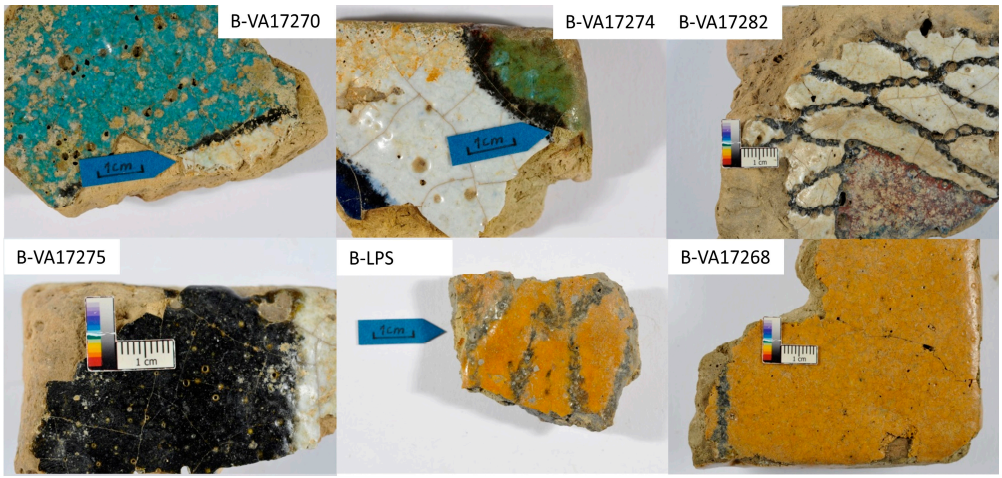


Figure 4. Photographs of the glazed brick fragments from Babylon selected for this study. © Vorderasiatisches Museum, SMB. All these fragments are dated from the reign of Nebuchadnezzar II (604–562 BC).

2.3. Instrumental Analysis

2.3.1. Microstructural Studies

The surface of the glazed bricks or glazed brick fragments were investigated under a digital microscope VHX-500FD (Keyence, Japan), and the polished cross-sections under a Zeiss Discovery V8 zoom microscope (Germany) for Aššur and Babylon bricks or a Nikon Eclipse LV100ND (Japan) for Khorsabad bricks. For Aššur and Babylon samples, the morphological study of the cross-sections was supplemented under Environmental Scanning Electron Microscopy (ESEM) (FEI Quanta 200 apparatus with ESEM capabilities, United States). For Khorsabad samples, the cross-sections were examined with a Jeol 7800F FEG SEM instrument (Japan). Both observations were performed at 15 kV or 20 kV in back-scattered electron mode (BSE).

2.3.2. Chemical Composition Studies

X-ray Fluorescence Spectroscopy (XRF)

Due to their heavy weathering, it is necessary for this article to present the XRF results for Aššur bricks that provide chemical information about their original colours. The X-ray beams were focused on the glaze surface with the help of a laser and a camera. Two-dimensional mappings were performed on some glazed bricks with an ELIO spectrometer (Bruker, Germany) mounted on a tripod and equipped with a motorized (XY) measuring head. The rhodium (Rh) X-ray tube was associated with a silicon drift detector (SDD) having an active area of 17 mm^2. The spot size was about 1 mm. The map step (distance between two measuring spots) varied from 1 mm to 2 mm. Each spot measurement was collected using the following setup: 50 kV, 50 µA current, 12 s, in air. Acquisition and evaluation of the XRF data were carried out using the ELIO software (XG Elio Software 1.6.0.1).

Point measurements were carried out in parallel to probe a larger number of Aššur glazes, using an ArtTAX Pro spectrometer (Bruker, Germany) equipped with a molybdenum (Mo) X-ray tube and polycapillary optics. The spot size was about 80 µm. The apparatus used a silicon drift detector (SDD) with an active area of 10 mm^2. Each point was analysed at 45 kV and 500 µA under He atmosphere. Acquisition and evaluation of the XRF spectra were carried out using a Spectra (Artax) 7.2.5 and a 7.4.0 software (Bruker AXS, Germany), respectively.

Scanning Electron Microscopy—Energy Dispersive X-ray Spectroscopy (SEM-EDX)

In parallel to the microstructural investigation of the polished cross-sections under ESEM, EDX analyses of Aššur and Babylon samples were performed with the QUANTAX system interfaced with the FEI Quanta 200 apparatus. Similarly, EDX analyses were performed on Khorsabad samples with the Quantax 400 Bruker system associated with

the FEG SEM. Both systems were calibrated using mineral standards. The analyses were undertaken at 20 kV or 15 kV accelerating voltage and 60 k/s as detector count rate. For the quantification of the glass matrixes, glazes were subjected to at least two map-scan to prevent the migration of the alkalis under the electronic beam, while inclusions were measured by several point analysis. Results were treated with the Bruker ESPRIT software using a Phi-Rho-Z quantification method.

The accuracy and consistency of the quantification have been verified by measuring glass standards.

For glass matrix, the concentrations of the analysed elements were converted into weight percent oxide (wt.%) and normalized to 100%. For pigments and inclusions, the concentrations were expressed as at.% and normalized to 100%.

Micro-Raman

The Raman spectra of Aššur and Babylon samples were acquired using a HORIBA XploRa confocal Raman microscope, using a doubled YAG laser emitting at 532 nm, associated with an Olympus (Japan) microscope, with a 1200 lines per millimetre grating and ultralow noise CCD detector. The Raman spectra of Khorsabad samples were measured using a RENISHAW Invia spectrometer with a 532 nm laser also, an 1800 lines/mm grating, and a Leica DM50 microscope. Usually, the measurements were taken with an optical objective of 50×. At the beginning of each series of measurements, the system was calibrated using the 520.5 cm^{-1} silicon line of a single crystal silicon wafer. The spectra were acquired with 5–10 accumulations of 10–60 s according to the fluorescence level of the samples.

2.4. Synthesis of Two Lead Antimonate Reference Compounds

Two lead antimonate compounds have been synthesized to help interpret the Raman spectra: pure $Pb_2Sb_2O_7$ and the solid solution close to composition $Pb_2Sb_{1.7}Fe_{0.3}O_{6.7}$, where Sb^{5+} is substituted by Fe^{3+} with an oxygen vacancy as charge compensation. Both powders were prepared by mixing appropriate amounts of PbO, Sb_2O_3, and Fe_2O_3 and heating the mixture in alumina crucible two times at 800 °C for 16 h in air, with an intermediate grinding of the powder to improve its chemical homogeneity. For pure $Pb_2Sb_2O_7$, 20 wt.% of NaCl was added to the mixture as a flux, according to the syntheses reported in the literature [35]. For the solid solution, the raw reagents have been weighted for a nominal amount of 0.8 Fe, and 1.2 Sb per formula unit, and no NaCl flux was used. The composition of the final $Pb_2Sb_{2-x}Fe_xO_{7-x}$ solid solution has been estimated by Rietveld analysis of the XRD diagram of the powder after the two heat treatments. A few crystalline by-products were also detected on the diagrams but could not be identified. The XRD diagrams and Rietveld analyses are given in the Supplementary Materials (Figure S4).

3. Results

3.1. The Black Colour

The XRF analyses did not find out any enrichment in Mn and Fe in the black colour of the present glazes (see, for instance, the 2D XRF mappings in Figures S1 and S2 in the Supplementary Materials), except the Aššur ones dated from the 9th century BC that is Mn-coloured (see, for instance, the 2D XRF mappings in Figure S3 in the Supplementary Materials), questioning the origin of this black. Microscopic examination by optical microscopy (Figure 5) and by SEM (Figure 6) reveals the presence of numerous nanoparticles in the glass matrix of Khorsabad and Babylon, which are optically black (MO images) with high electronic density (they are white on the SEM images). Note that for the black glaze of brick fragment B-VA17275, these nanoparticles were observed in lesser quantities compared to the other Babylon blacks, and this glaze, devoid of quartz-like inclusions, appears slightly translucent with a blackish-dark green hue in some areas. The diameters of these spherical particles range between 50 and 600 nm with a few bigger particles, which, for example, left the holes in the Figure 6b,c images. These holes were induced by the polishing and implied poor adherence of these particles with the surrounding glass.

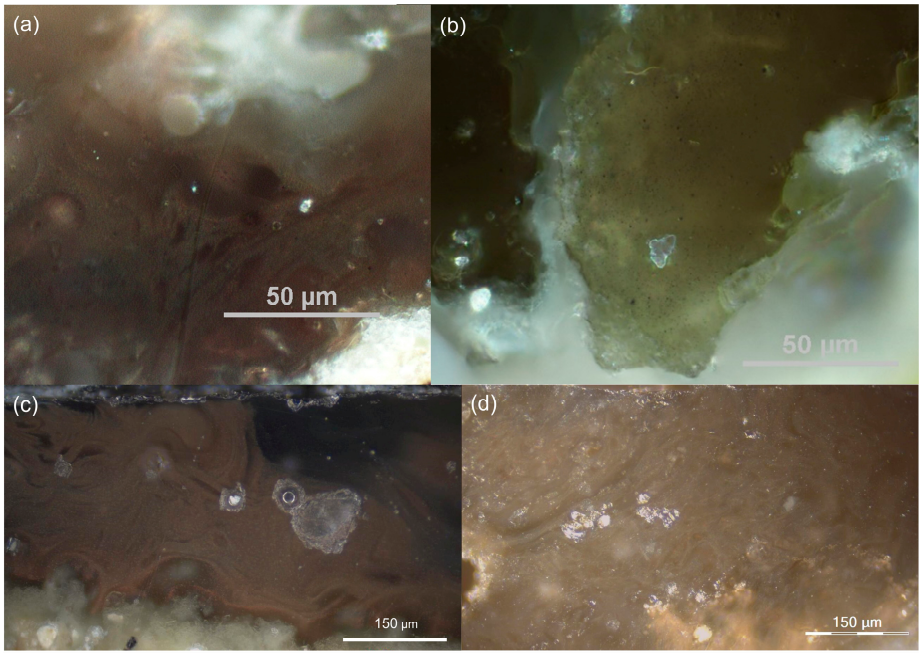


Figure 5. Optical Microscopy images of the black samples taken from Khorsabad bricks K-N8099 (**a**) and K-N8080 (**b**), and from Babylon bricks (polished cross-sections) B-VA17274 (**c**) and B-VA17282 (**d**). The blackness of the particles is more visible on the (**b**) image of a glass protusion captured in transmitted light. In the other images only taken in reflecting light, the clouds of particles appear brown because they provoke the scattering of white light.

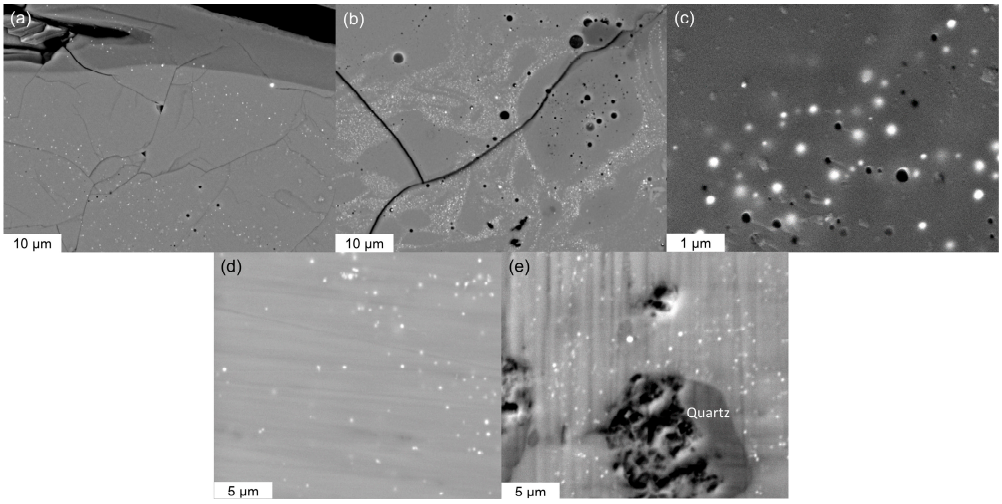


Figure 6. SEM images in Backscattered Electron mode (BSE) of the polished black samples taken from Khorsabad bricks (**a**) K-N8098 and (**b**,**c**) K-N8099 and from Babylon brick (**d**) B-VA17274 and (**e**) B-VA17282.

EDX analysis was performed by point analysis on the biggest particles. The results were averaged by excluding the spectra with the highest Si contamination, as Si is assumed not to enter the composition of the particles. These analyses reveal that the particles are essentially copper sulphides. As an example, we report in Table 1 the averaged result for Khorsabad black glaze K-N8098 and the composition of the surrounding glass matrix for comparison. It should be noted that the content of the glass matrix in Pb and Sb was always below the limit of detection and very close to it for S, Cu, and Fe. Thus, there is a clear distinction between the copper sulphide particles and the glass matrix that bears only traces of S, Cu, and Fe. For the same black glaze of Khorsabad or Babylon, we found

one composition of copper sulphide particles among three distinct types: (i) S and Cu only; (ii) S, Cu as major elements and Pb as minor element with traces of Fe; (iii) S, Cu as major elements and Fe, Pb, Sb as minor elements. These different ranges of impurities are probably related to different copper sulphide-bearing raw materials. The complete and detailed study of the particle compositions and stoichiometries is out of the scope of this article and will be presented elsewhere.

Table 1. Average EDX analyses (at.%) of the copper sulphide nanoparticles in one black sample of Khorsabad investigated in this study (standard deviations in grey). The last column gives the metal/sulphur atomic ratio. loq: limit of quantification.

Sample	Si	S	Cu	Fe	Pb	Sb	(Cu + Pb + Sb + Fe)/S
K-N8098	21.16	5.04	1.95	0.82	0.57	0.67	0.8
Sigma	1.38	1.65	0.94	0.32	0.32	0.52	
K-N8098 Glass Matrix	26.69	0.22	<loq	0.22	<loq	<loq	
Sigma	0.46	0.05		0.03			

It was possible to attain good quality Raman spectra of these black glazes because their low level of alteration minimized the fluorescence phenomena. Representative Raman spectra are shown in Figure 7. The major contribution to these spectra is the glass matrix, revealed by the bands around 1100 cm^{-1} and 500–650 cm^{-1} assigned to the elongation and deformation vibrations of the silicate network, respectively. The main feature not belonging to the glass matrix is the wide peak at 420 cm^{-1} and a shoulder at around 375 cm^{-1}, which is systematic and characteristic of these black glazes. We examined the Raman spectra of various copper sulphides available in the online RRUFF database, but none of them showed any main peak at 420 cm^{-1}. The nanometric size of these particles and their embedded situation in the glass may strongly modify the vibrational spectrum from that of the bulk phase, impinging their clear identification in the Raman spectra. More likely, we propose that the 420 cm^{-1} peak and its shoulder are related to the Fe^{3+}-S^{2-} chromophore because very similar Raman features appear in spectra of numerous black glazes that are coloured by this chromophore [36,37]. Additionally, the Raman spectra show a distinctive band at about 990 cm^{-1}, which is assigned to the symmetric stretching of sulphate groups [38]. Therefore, sulphur in the redox state +VI is also present in the glass matrix. Since coexistence of the +VI and the −II redox states for S in the same glass region is unlikely for thermodynamic reasons, we suppose that the glass may be inhomogeneous on the micrometre scale, which is the scale of the Raman analyses, with some areas bearing S^{2-} and the amber chromophore, and some other areas showing complete oxidation of S as SO_4^{2-} units.

For the black glazes of Aššur dated from the 8th–7th century BC (not Mn-coloured), copper sulphide nanoparticles were not observed within the mass of silica gel that results from the strong weathering of these glazes. By SEM-EDX analysis, we have identified instead very few nanoparticles rich in Ag and S within the black glaze of brick A-810791, for which the element Ag was detected by XRF analysis. This seems to concern a reduced number of bricks according to a large survey by XRF spectroscopy, and the role of these nanoparticles in the black colour cannot be established. Note that the blackness of these glazes appears much less intense than that of the 9th century BC (Mn-coloured) (Figure 3). Moreover, as stated before, the black glazes dated from the 8th–7th century BC displays nearly always whitish areas that we associate with a decolouration phenomenon. Therefore, we suppose that the white contour lines of this corpus, for which no colouring oxide could be detected, are the result of extreme cases of weathering of glazes that were originally black.

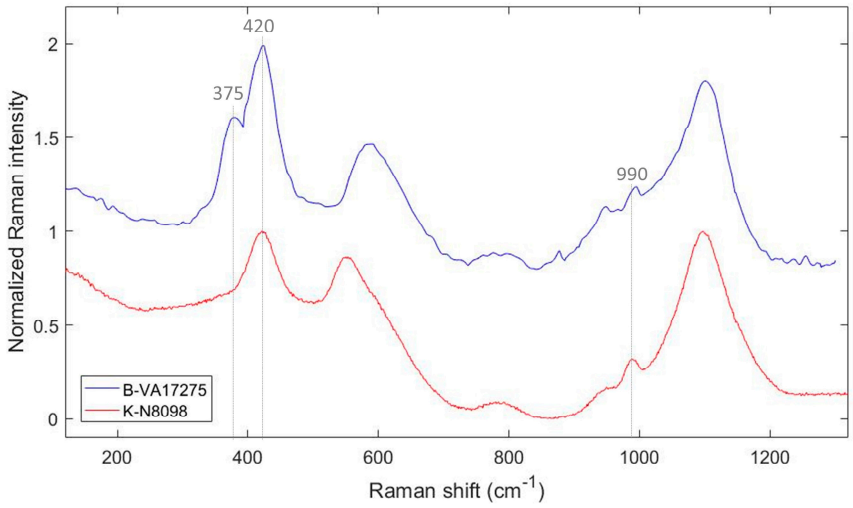


Figure 7. Raman spectra of the copper sulphide particles and glass matrix in the black samples of bricks from Khorsabad (K-N8098) and from Babylon (B-VA17275).

3.2. The Orange–Yellow Colour

In this part, we describe the composition and microstructure of the inclusions within the orange–yellow glazes, first of Khorsabad and Babylon, then of Aššur that is a more complicated case due to the strong alteration of the glazes and to the coexistence of various yellow hues. The antimonates existing in these glazes are diverse, especially the lead antimonate of pyrochlore structure. Their investigation by EDX analysis and Raman spectroscopy is reported in the last paragraph.

3.2.1. The Orange–Yellow Colour of Khorsabad and Babylon

The microstructures of the orange–yellow glazes of Khorsabad and Babylon are very similar in their main features. A transparent, very slightly honey-coloured glass matrix contains a high number of large inclusions, typically 50 to 100 µm wide, of pigment with a variety of colours in the white–yellow–orange palette. These pigment inclusions all consist of assemblies of finely divided crystals, of which size is the order of 1 µm. They are unevenly distributed in the glass. Their microstructure and irregular distribution strongly suggest an ex situ technique for the fabrication of these glazes, consisting of the ex situ preparation of the pigments and their mixing with glass frit or with a glass-forming mixture. Similar to ancient Egypt and Rome [24,29], lead antimonates from the ancient Near East were indeed probably mostly prepared ex situ [14], although examples of possible in situ crystallization during the firing of the glaze are also reported [12].

Khorsabad glazes bear antimonates and hematite (Fe_2O_3) as major and minor pigment inclusions, respectively. It was possible to distinguish five types of colours and the chemistry of the antimonates, which are depicted in Figure 8. At first, on the right-hand side of Figure 8b, a big "bunch of grapes" inclusion of Ca-antimonate, white in colour, represents one minor type of antimonate. Then, Figure 8a–c shows the three major types of antimonates, all are lead-antimonates with various colours and impurities. These types are named according to their optical colour: Pale Yellow (PY), Dark Yellow (DY), and Orange–Red (O–R). At last, Figure 8d shows the fifth type of antimonate, of the Orange–Brown colour (O–B). Its grey contrast on the BSE image comparatively to the white lead-antimonates is due to the fact that it is not a lead-antimonate but an iron-antimonate.

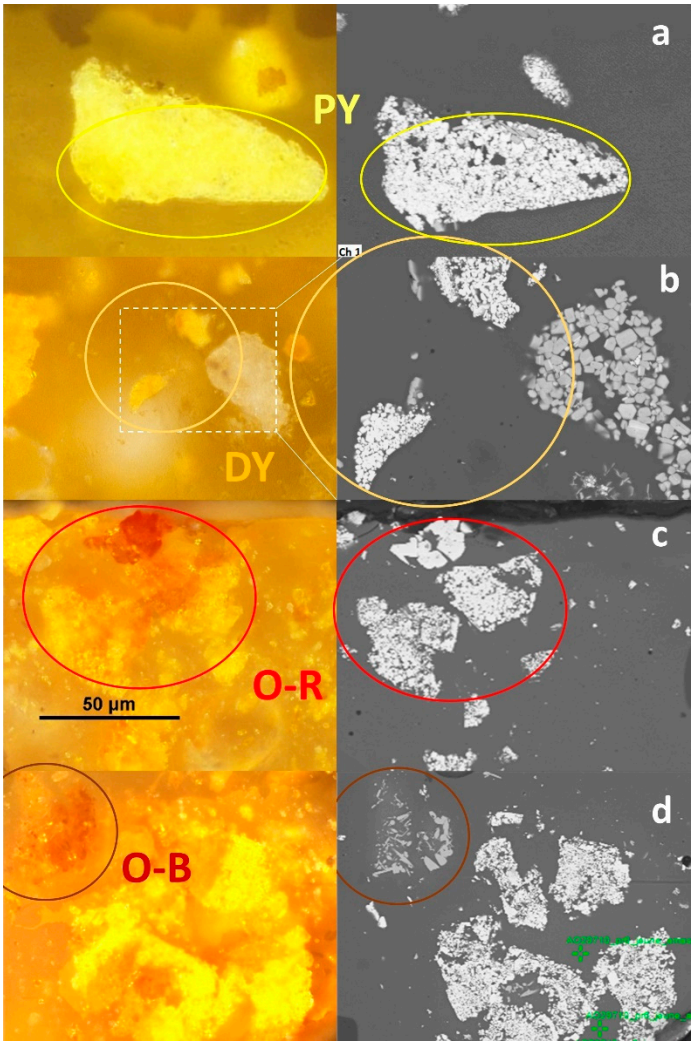


Figure 8. Optical microscopy (OM) and SEM in back-scattered electron mode (BSE) of the five types of antimonates found in the orange–yellow glazes of Khorsabad bricks: (**a**) K-N8105, (**b**) K-N8080, (**c**) K-AO29710, first area, (**d**) K-AO29710, second area. Four colours of the orange–yellow palette are associated to these antimonates: Pale Yellow (PY), Dark Yellow (DY), Orange–Red (O–R) and Orange–Brown (O–B). From EDX and Raman spectroscopy, PY, DY and O–R are lead antimonates with the pyrochlore structure, while O–B are iron antimonates with stoichiometry 1:1 for Fe_2O_3: $Sb_2O_3/5$ and unidentified structure. On the right-hand side of the (**b**) images, the white colour is also present and associated to calcium antimonates with $CaSb_2O_6$ structure, having two different morphologies: cubic crystals in the "bunch of grapes" and needle-like crystals (see at the bottom of the "bunch").

In the orange–yellow glazes of Babylon (Figure 9), three different types of lead-antimonates were also observed. They are named PY, DY, and O–R according to their Pale Yellow, Dark Yellow, and Orange–Red optical colour and similar to the above description for Khosabad glazes. DY antimonates are clearly the most numerous in the orange–yellow glazes of Babylon, and PY the least. In addition, the area covered by the optical microscopy image contains a small red hematite inclusion marked with R. Hematite inclusions are present in the Babylon orange–yellow, although not as abundant as in the Khorsabad orange–yellow. This may be related to the macroscopic observation that, concerning the orange–yellow colour, Babylon glazes are slightly more yellow while Khorsabad glazes are slightly more orange. In photographs, the b colour coordinate is systematically higher for Babylon than for Khorsabad. Thus, this colour will be referred to as yellow for Babylon and orange for Khorsabad in the following.

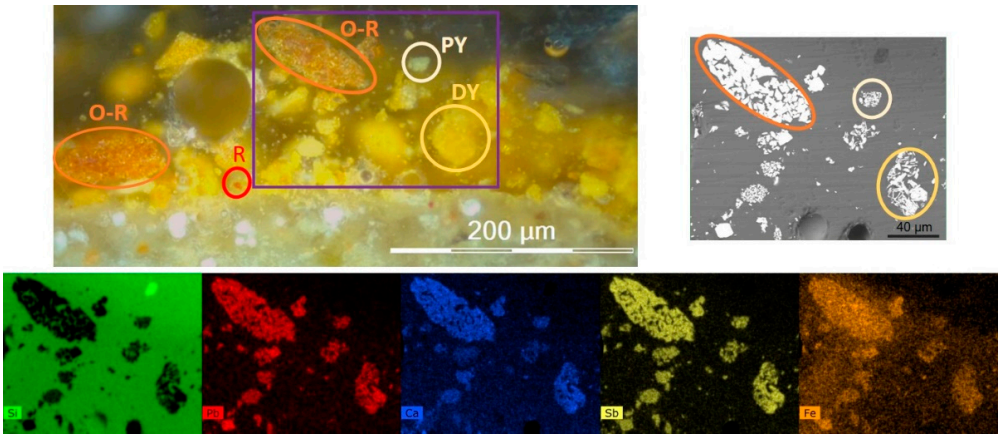


Figure 9. Optical Microscopy image (top left), SEM in back-scattered electron mode (BSE) image (top right) and EDX cartography (bottom—from left to right: Si, Pb, Ca, Sb, Fe elements) of the polished yellow sample from brick B-LPS showing the three types of antimonates found in the orange–yellow glazes of Babylon bricks. The violet rectangle on the Optical Microscopy shows the area of the BSE-image analysed by EDX for the cartography. Three colours of the orange–yellow palette are associated to these antimonates: Pale Yellow (PY), Dark Yellow (DY), Orange–Red (O–R). From EDX and Raman spectroscopy, they are lead antimonates with the pyrochlore structure. On the Optical Microscopy image, a fine particle of red hematite (µ-Raman result) is also highlighted (R).

These three types of lead-antimonates have been characterized by EDX analyses and Raman spectroscopy, which confirmed their distinctness and their good correspondence between Khorsabad and Babylon. This will be reported in the last paragraph.

Note that contrary to Khorsabad, we did not observe the presence of Ca-antimonates, neither as cubic crystals nor as needles.

Moreover, the pigment inclusions generally show many signs of chemical reactivity with the glass phase during the firing and cooling of the glaze. This reactivity is out of the scope of this paper, although it promises a wealth of information on the thermochemical conditions of preparation of these materials. Figure 10 shows several typical cases of reactivity in a Khorsabad glaze, with the aim to mention it for further studies. Three zones are highlighted in the area covered by the optical microscopy image:

(1) Zone (1) contains a hematite inclusion surrounded by a lead antimonate inclusion shaped as a croissant. In the magnified BSE image of the lead antimonate crystals, a chemical contrast can be observed with greyer crystals on the side of hematite. From EDX mapping of this area (not shown), this bright/grey contrast is due to lead/calcium substitution within the crystals;

(2) Zone (2) corresponds to a large inclusion of calcium antimonate (grey "bunch of grapes" shaped inclusion, already shown in Figure 8b) laid next to two smaller inclusions of lead antimonates (white on the BSE image). The magnified BSE image of these Ca-antimonates show that some crystals are crossed from side to side by white Pb-rich lines;

(3) Zone (3) is very complex with iron enrichment in the left-centre of the zone, although no hematite crystal can be discerned. On this left-centre zone, a bow of lead antimonates surrounds long needle-shaped crystals of Ca-antimonates, the morphology of the latter suggesting that they have formed by precipitation and growth. The internal antimonate crystals of the bow are strongly Ca-enriched. On the right-centre zone, four small inclusions of lead antimonate are visible, displaying different shades of yellow on the optical microscopy image. Two inclusions at the bottom are dark yellow and Fe-enriched, while the larger inclusion on the right is pale yellow and Ca-enriched. This latter inclusion even bears white Ca-antimonate crystals on the top of it.

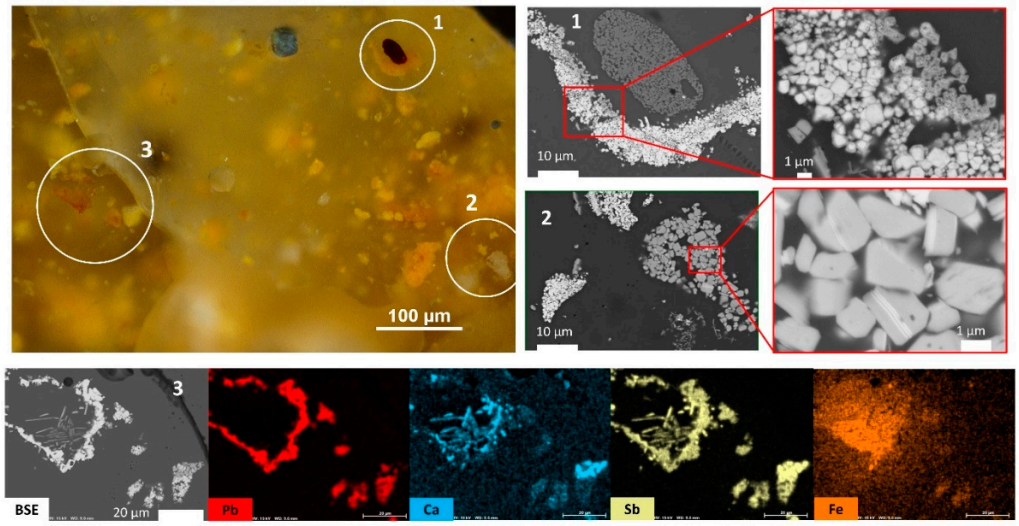


Figure 10. Optical Microscopy image (top left), SEM in back-scattered electron mode (BSE) images (top right and bottom left) and EDX cartography (bottom—from left to right: Pb, Ca, Sb, Fe elements) of the polished orange sample from brick K-N8080. Three zones are distinguished and depicted by SEM in back-scattered electron mode (BSE): (1) A hematite crystal group (dark grey) surrounded by a Pb-antimonate group (white) with Ca enrichment (light grey). (2) A large Ca-antimonate group (light grey) whose crystals show white Pb-enriched lines and two small Pb-antimonate groups (white). At the bottom of the large Ca-antimonate group, needle-shaped Ca-antimonate crystals are visible. (3) A large and complex group of crystals with Pb-antimonates (white on the BSE image) surrounding Ca-antimonate needle-shaped crystals (grey) in a Fe-rich area. At the bottom-right of the image, four small Pb-antimonate groups can be distinguished. The biggest one on the right also contains Ca-antimonate cubic crystals. The three others are slightly Fe-enriched.

3.2.2. The Orange–Yellow Colour of Aššur

Under Optical Microscopy, coloured inclusions from a few tens of micrometres up to about 200 micrometres can be distinguished on the surface of the weathered orange–yellow glazes from Aššur. By SEM-EDX and Raman analysis (detailed in the next paragraph), these inclusions were associated with Pb-antimonates opacifiers. Based on their colours within the same glaze, we have distinguished three different shades in the orange–yellow palette (Figure 11): (i) Orange: orange–red (O–R) inclusions in the majority (and fewer inclusions in dark yellow shades); (ii) Yellow: Dark Yellow (DY) inclusions in the majority (and fewer inclusions in orange shades); (iii) Pale yellow (with a greenish accent): Pale Yellow (PY) inclusions in the vast majority. Thus, Optical Microscopy was a very useful tool for assigning a colour to glazes that appear strongly discoloured to the naked eye.

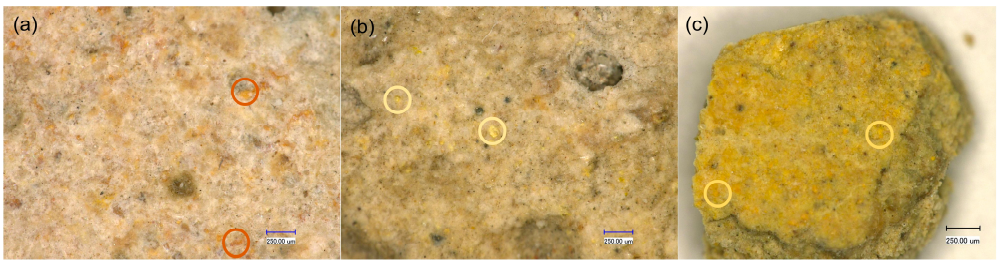


Figure 11. Optical microscopy (OM) of the surface of weathered glazes from Aššur showing (**a**) Orange–Red (O–R) particles in the orange glaze of brick A-811251, (**b**) Pale Yellow (PY) particles in the pale-yellow glaze of brick A-811251, (**c**) Dark Yellow particles (DY) in the yellow glaze of brick A-812093. Some of these particles are marked on the images by a coloured circle. The scale bar is 250 µm.

Note that for the pale-yellow glazes, the greenish shade was very often observed for the whitish weathered material surrounding the inclusions. Additional low levels of copper higher than for the orange and yellow glazes are detected by XRF (Figure 12). It is almost impossible to know whether the copper was originally present in a higher amount but was partially leached during weathering so that the greenish accent could have been more pronounced. Note that the archaeologists had distinguished these glazes from the other orange–yellow ones by the mention "weingelb" i.e., "wine yellow" on the drawings of the glazed facades excavated during their archaeology expedition to Aššur in the early 20th century, suggesting a greenish accent.

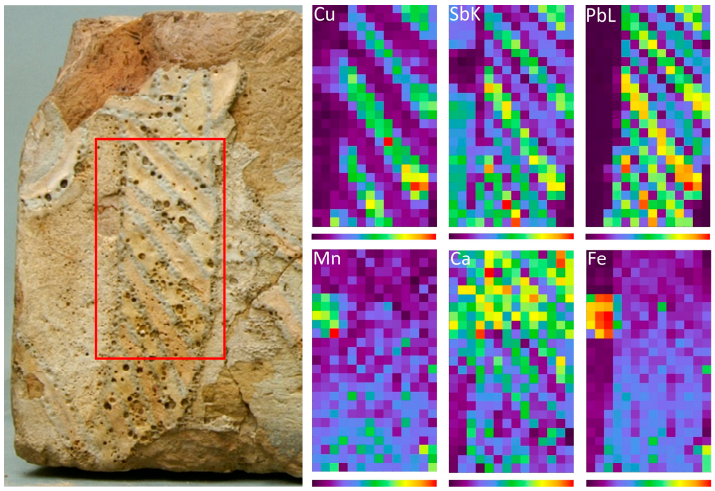


Figure 12. XRF Cartography of a glazed area of the A-811452 brick from Aššur (area marked with a red rectangle on the left image) displaying an alternation of orange and pale greenish–yellow glazes separated by a contour line (originally supposed to be black).

Under SEM, these coloured inclusions are shown to be clusters of microcrystals (SEM images in Figures 13–15). Their microstructure does not appear well defined at the SEM scale, and we cannot exclude that these pigments have evolved over time because of the heavy weathering of the glazes. Their dispersion is rather heterogeneous, which would speak for an ex situ preparation as already pointed out before for the yellow–orange glazes of Babylon and Khorsabad. As for Babylon, no white Ca-bearing antimonate was observed within these orange–yellow glazes.

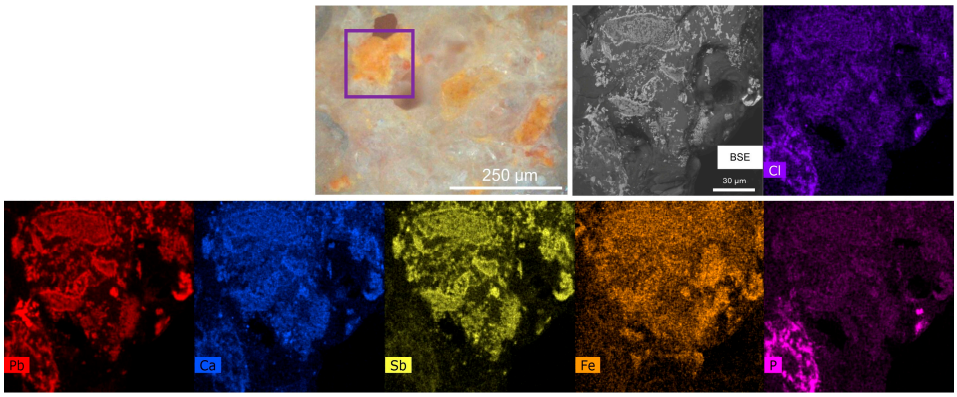


Figure 13. Optical microscopy (OM) image (top left), SEM in back-scattered electron mode (BSE) image (top-middle) and EDX cartography (top right—Cl element—and bottom—from left to right: Pb, Ca, Sb, Fe and P elements) of a polished cross-section of the weathered orange glaze of brick A-811251 showing the presence of orange–red lead antimonates, and Pb-P-Cl rich phases. The violet rectangle on the OM image shows the area of the SEM-EDX analysis.

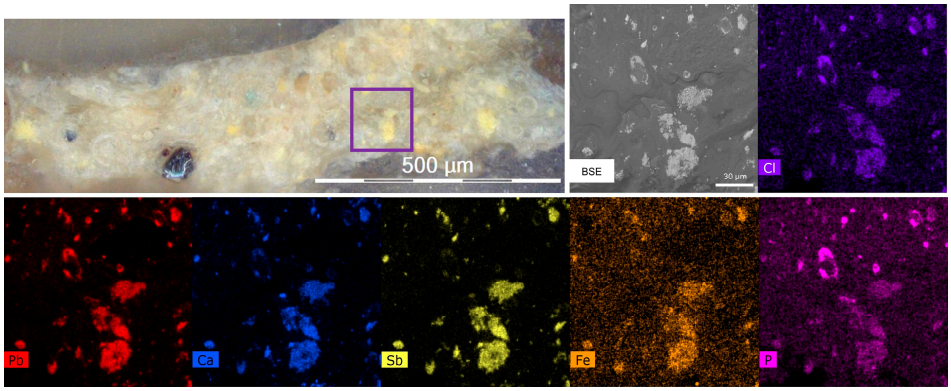


Figure 14. Optical microscopy (OM) image (top left), SEM in back-scattered electron mode (BSE) image (top-middle) and EDX cartography (top right—Cl element—and bottom—from left to right: Pb, Ca, Sb, Fe and P elements) of a polished cross-section of the weathered pale yellow glaze of brick A-811251 showing the presence of pale yellow lead antimonates, and Pb-P-Cl rich phases. The violet rectangle on the OM image shows the area of the SEM-EDX analysis.

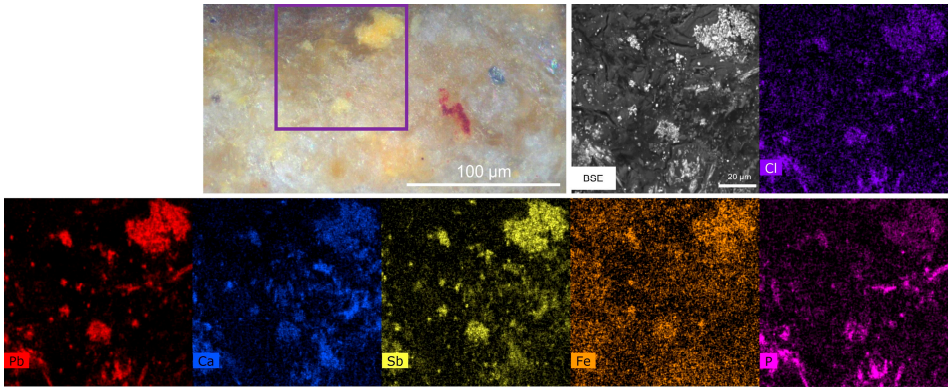


Figure 15. Optical microscopy (OM) image (top left), SEM in back-scattered electron mode (BSE) image (top-middle) and EDX cartography (top right—Cl element—and bottom—from left to right: Pb, Ca, Sb, Fe and P elements) of a polished cross-section of the weathered yellow glaze of brick A-812093 showing the presence of dark yellow lead antimonates and Pb-P-Cl rich phases. The red inclusion on the OM image was identified as hematite (µ-Raman). The violet rectangle on the OM image shows the area of the SEM-EDX analysis.

Red hematite was discriminated in the yellow sample of brick A-812093 (Figure 15). Other inclusions were found in the weathered glazes of Aššur, whatever their colour, such as quartz, calcite, gypsum (SEM-EDX and µ-Raman results). Specificity of the orange–yellow glazes is the systematic presence of inclusions rich in Pb, P, and Cl elements for which no satisfying Raman signal could be collected. They could be pyromorphite-type phases ($Pb_5(PO_4)_3Cl$) with a low degree of crystallisation. It is supposed that these phases have been formed during the ground deposit period by the reaction of the lead from the glaze with phosphates and chlorides from the soil. Note that pyromorphite has been evidenced in weathered yellow glazes from Borsippa and Nimrud [8].

3.2.3. Compositional Analysis of the Lead Antimonate by EDX and Raman

As described in the previous paragraph, three types of lead antimonates have been distinguished according to their colour in optical microscopy images, namely Pale Yellow (PY), Dark Yellow (DY), and Orange–Red (O–R) antimonates. To understand the origin of their colour, these three groups have been distinctly characterized by EDX and Raman. Their cationic ratio (by EDX) and their Raman vibrational spectra allow assigning all three types to the pyrochlore structure of general stoichiometry $A_2B_2O_7$, with A being mainly

Pb^{2+} and B being Sb^{5+}. It is important to emphasize that this fluorite-related crystalline structure is adopted by many compounds and solid solutions, as it can withstand numerous chemical substitutions. It belongs to the cubic system with space group $Fd\bar{3}m$. With respect to the fluorite structure, half of the cationic sites are SbO_6 octahedra (Sb in 48f position), sharing three edges and forming SbO_6 chains along the face diagonals of the pyrochlore cubic cell. The other half of cationic sites are distorted PbO_8 polyhedra (Pb in 48f) bearing six equatorial oxygens (O1 in 48f) and two axial oxygens at a larger Pb-O distance (O2 in 8b). Contrary to the fluorite structure, the 8a site is vacant (no oxygen). Every PbO_8 polyhedron shares one axial oxygen (O2) with three other PbO_8, forming large Pb_4O tetrahedra (the 8b position of the O2 has Td symmetry).

The EDX analyses of the lead-antimonates have been averaged according to their type or colour, for Khorsabad, Babylon, and tentatively for Aššur, in Table 2. For the well-conserved glazes of Khorsabad and Babylon, the contribution of the glass matrix has been estimated by normalizing the average composition of the glass matrix of orange–yellow glazes (described later in this article) to the Si contamination value measured in the antimonates (about 2 at.% of Si). This contribution is necessary to assess the insertion of Ca and Fe in the pyrochlore structure because these two elements are also contained in the glass matrix.

Table 2. Average EDX analyses (at.%) performed on lead antimonates and iron antimonates as distinguished by their colours in optical microscopy for the three archaeological sites Khorsabad, Babylon and Aššur (standard deviation in grey). For every of the two archaeological sites Khorsabad, resp. Babylon, the last blue line gives the estimated contribution of the glass matrix in the DY colour, resp. PY colour, by taking the average composition of the glass matrix measured in the orange sample, resp. the yellow samples and normalizing it to 2 at.%, resp. 2.24 at.% Si. loq: limit of quantification. * For Aššur, the interpretation of these analyses is limited by the non-negligible contribution of the surrounding matrix, which was systematically obtained in the measured spectra.

Archeological Site	Pigment Colour		O	Si	Na	Mg	K	Al	Cl	Ca	Fe	Pb	Sb
Khorsabad	O–R	Mean	55.53	<loq	0.59	<loq	<loq	0.55	0.49	4.03	5.13	15.64	17.41
		Sigma	0.09		0.31			0.00	0.06	0.64	0.87	0.62	0.26
	DY	Mean	55.28	2.00	2.13	0.77	<loq	0.61	0.30	2.43	3.56	17.15	15.73
		Sigma	0.25	2.25	1.25	1.10		0.22	0.01	0.57	2.25	2.61	0.37
	PY	Mean	54.99	2.34	3.35	0.88	<loq	0.83	0.28	3.73	2.45	15.25	15.90
		Sigma	0.49	1.24	0.69	0.16		0.18	0.11	0.79	0.52	2.04	0.83
	O–B	Mean	59.41	2.31	1.40	0.22	<loq	0.22	<loq	1.75	17.70	0.10	16.74
		Sigma	0.10	1.66	0.63	0.03		0.09		0.14	0.87	0.05	1.56
	Glass Matrix 2% at Si	Mean	-	2.00	0.76	0.10	0.11	0.04	0.03	0.11	0.07	0.05	0.02
Babylon	O–R	Mean	54.99	<loq	1.02	0.93	<loq	0.80	0.31	3.52	3.76	17.68	16.92
		Sigma	0.29		0.50	0.33		0.38	0.03	0.88	1.05	1.06	0.56
	DY	Mean	54.83	<loq	1.02	0.63	<loq	0.36	0.39	2.45	3.44	19.61	17.22
		Sigma	0.17		0.33	0.22		0.11	0.21	1.03	1.05	1.44	0.98
	PY	Mean	54.89	2.24	3.43	1.53	<loq	1.12	0.27	2.87	1.79	15.67	16.15
		Sigma	0.09	0.72	1.04	0.20		0.05	0.17	0.32	1.15	1.18	0.42
	Glass Matrix 2.24% at Si	Mean	-	2.24	0.91	0.22	0.15	0.07	0.03	0.16	0.03	0.07	0.02
Aššur *	O–R	Mean	57.19	6.98	1.41	0.73	0.17	0.65	0.26	1.51	4.45	14.82	11.81
		Sigma	0.21	0.86	0.78	0.26	0.12	0.14	0.07	0.18	0.27	1.23	1.33
	DY	Mean	55.76	4.81	2.38	1.24	0.28	1.63	0.67	3.20	3.11	14.23	12.69
		Sigma	0.17	0.55	0.56	0.26	0.07	0.08	0.27	0.83	0.20	1.52	0.37
	PY	Mean	57.48	9.33	2.94	1.20	0.19	1.45	0.45	4.20	1.42	8.94	12.42
		Sigma	0.23	0.38	0.42	0.36	0.09	1.12	0.14	1.55	0.48	1.71	0.99

First, it is clear from Table 2, and the comparison with the glass matrix contribution that Na, Mg, Al, Ca, and Fe elements enter the pyrochlore structure. Among these elements, Ca and Fe enters in a minor but not negligible amount with respect to the main Pb and Sb cations. Mg and Al enter the pyrochlore as minor elements that will be neglected in the following. Concerning Na, its contribution is not negligible, especially in the PY antimonates for which the Na content is close to the Ca content.

To obtain the composition of the pyrochlore formula unit and the type of chemical substitutions, the at.% of the main cations, Pb^{2+}, Sb^{5+}, Ca^{2+}, and Fe^{3+}, have been normalized to a total of four as in $A_2B_2O_7$. The numbers are given in Table 3. For Khorsabad, the orange–brown antimonates (O–B) are also included in the table, although they are actually iron-antimonates, with a Fe/Sb ratio close to 1. Table 3 also reports the (Pb + Ca)/(Sb + Fe) ratio and the Pb/Sb ratio in the last two columns. As expected according to the sizes and valency states of the cations, the (Pb + Ca)/(Sb + Fe) ratio is close to one (except for Khorsabad O–R), which indicates that Ca^{2+} ions substitute for Pb^{2+} and Fe^{3+} for Sb^{5+} in the pyrochlore structure. Note that the valency state of Fe is assumed to be +3 in the pyrochlore, considering the equilibrium with the +5 valency for Sb. The presence of hematite in the vicinity of the antimonates also points out an oxidized state for these glazes.

Table 3. Composition of the lead antimonate $Pb_2Sb_2O_7$ in PY, DY and O–R colours for the three archaeological sites Khorsabad, Babylon and Aššur by normalizing the Pb + Ca + Sb + Fe atomic content to 4 (standard deviation in grey). The second to last column gives the (Pb + Ca)/(Sb + Fe) ratio to verify the hypothesis that Ca^{2+} substitutes Pb^{2+} and Fe^{3+} substitutes Sb^{5+} in the pyrochlore structure (neglecting the contribution of Na^+, Mg^{2+} and Al^{3+} ions). The last column gives the Pb/Sb ratio to compare with existing analyses in the literature. For Khorsabad, resp. Babylon, the last blue line gives the average composition of the DY colour, resp. of the PY colour corrected from the estimated contribution of the glass matrix, by subtracting to the DY Mean line in Table 2. * For Aššur, the interpretation of these analyses is limited by the non-negligible contribution of the surrounding matrix, which was systematically obtained in the measured spectra.

Archeological Site	Pigment Colour		Pb	Ca	Sb	Fe	(Pb + Ca)/(Sb + Fe)	Pb/Sb
Khorsabad	O-R	Mean	1.48	0.38	1.65	0.49	0.87	0.90
		Sigma	0.04	0.07	0.05	0.08		
	DY	Mean	1.76	0.25	1.62	0.37	1.01	1.11
		Sigma	0.10	0.07	0.12	0.09		
	PY	Mean	1.63	0.40	1.71	0.26	1.03	0.95
		Sigma	0.16	0.11	0.09	0.06		
							Fe/Sb	
	O–B	Mean	0.01	0.19	1.84	1.95	1.06	
		Sigma	0.01	0.01	0.05	0.05		
							(Pb + Ca)/(Sb + Fe)	
	DY corrected	Mean	1.77	0.24	1.63	0.36	1.01	1.11
Babylon	O–R	Mean	1.69	0.33	1.62	0.36	1.02	1.04
		Sigma	0.14	0.08	0.04	0.10		
	DY	Mean	1.84	0.23	1.61	0.32	1.07	1.14
		Sigma	0.11	0.08	0.09	0.08		
	PY	Mean	1.72	0.32	1.78	0.19	1.03	0.97
		Sigma	0.05	0.05	0.12	0.12		
	PY corrected	Mean	1.72	0.30	1.78	0.19	1.02	0.97
Aššur *	O–R	Mean	1.82	0.19	1.45	0.55	1.00	1.26
		Sigma	0.09	0.05	0.03	0.08		
	DY	Mean	1.71	0.39	1.53	0.37	1.10	1.12
		Sigma	0.13	0.12	0.02	0.03		
	PY	Mean	1.33	0.62	1.84	0.21	0.95	0.72
		Sigma	0.27	0.22	0.09	0.07		

The PY inclusions may be a distinct case because of the high content in Na that is close to the Ca one. The formula unit of Babylon PY considering Na in addition to Ca and Fe is given in Table 4. The formula unit for Khorsabad PY is similar. According to this formula unit composition, the type of cationic site hosting Na^+ ion is not obvious, as the (Pb + Ca + Na)/(Sb + Fe) ratio is significantly higher than 1. Na^+ ions may possibly enter other available sites in the pyrochlore structure, such as interstitial sites.

Table 4. Composition of the lead antimonate $Pb_2Sb_2O_7$ in Babylon PY, by normalizing the Pb + Ca + Na + Sb + Fe atomic content to 4. The blue line is corrected from the contribution of the glass matrix.

Pigment Colour	Pb	Na	Ca	Sb	Fe	(Pb + Ca + Na)/(Sb + Fe)	Pb/Sb
PY	1.57	0.34	0.29	1.62	0.18	1.22	0.97
PY corrected	1.61	0.26	0.28	1.67	0.18	1.16	0.97

The three types, or colours, of the lead antimonates, correspond to different concentration ranges of chemical substitutions. The Pale Yellow (PY) is a lead antimonate particularly enriched in Ca and Na. The Dark Yellow (DY) is slightly poorer in Ca but richer in Fe, with a remarkably homogeneous Fe content (according to the s.d. value) of about 0.32–0.37 per formula unit. The Orange–Red (O–R) is more complicated to define because the content in Ca and the cationic ratio are more diverse, but in all three cases, the Fe content is the highest, from 0.36 to 0.55 per formula unit. As we will see later, the Raman spectra of the O–R antimonates bear the main features of the pyrochlore structure, except for an additional large band at about 630 cm^{-1}. By optical microscopy, O–R inclusions are always observed in red areas so that the inclusion and its red area produce an orange–red stain (this is well visible in the orange glaze cross-section of Khorsabad in Figure 8 and in the Aššur microscopy image of Figure 13). Therefore, it is possible that the high Fe content stems from contamination of the analysis by the immediate environment of the antimonate that is red and very likely Fe-enriched. The 630 cm^{-1} could be a signature of this iron oxide-rich medium.

The Raman spectra are shown in Figure 16, according to the colour and the corpus. In order to help their interpretation, powders of pyrochlore lead antimonates with $Pb_2Sb_2O_7$ composition and $Pb_2Sb_{1.7}Fe_{0.3}O_{6.7}$ composition have been synthesized in the laboratory and used as references. Their Raman spectra are depicted in Figure 17.

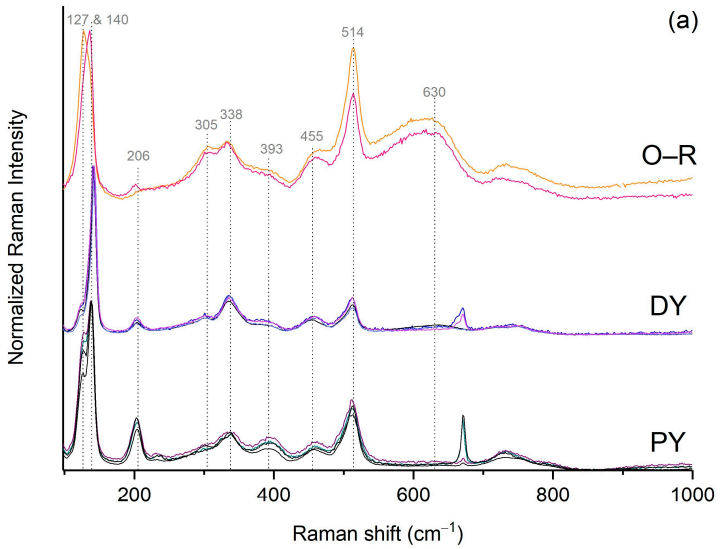


Figure 16. *Cont.*

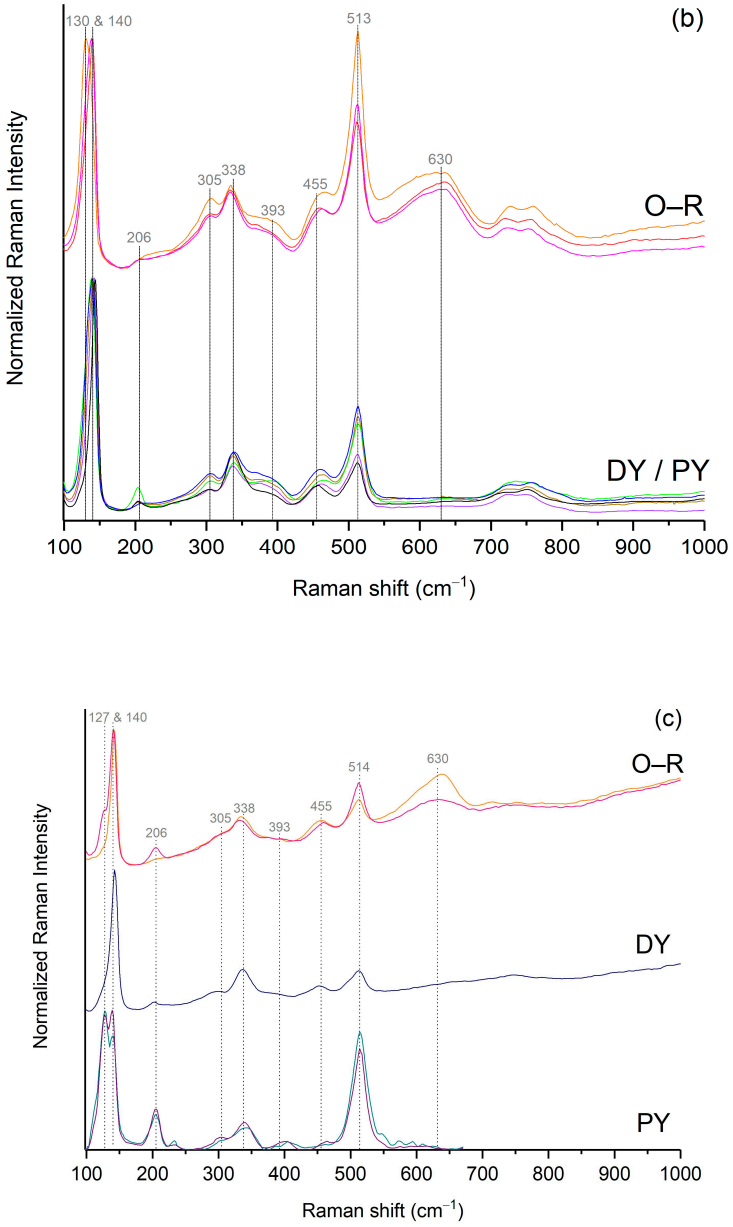


Figure 16. Raman spectra of the various Pb-antimonates in the orange glazes of bricks from (**a**) Khorsabad, (**b**) Babylon and (**c**) Aššur, for the different colours depicted by optical microscopy: Orange Red (O–R), Dark Yellow (DY) and Pale Yellow (PY). (**a**) The presented O–R spectra are taken from bricks K-AO29710 and K-N8123; DY and PY spectra are taken from bricks K-N8105. (**b**) The presented O–R, DY/PY spectra are taken from bricks B-VA17268 and B-LPS. (**c**) The presented (O–R) and (PY) spectra are taken from brick A-811251, the DY spectrum is taken from brick A-812093. All the spectra have been normalized to the intensity of the peak at 140 cm^{-1}. The peak at 671 cm^{-1} is assigned to calcium antimonates $CaSb_2O_6$. The peak at around 630 cm^{-1} is possibly a contribution of the Fe oxide-rich environment of the lead antimonates in the O–R areas.

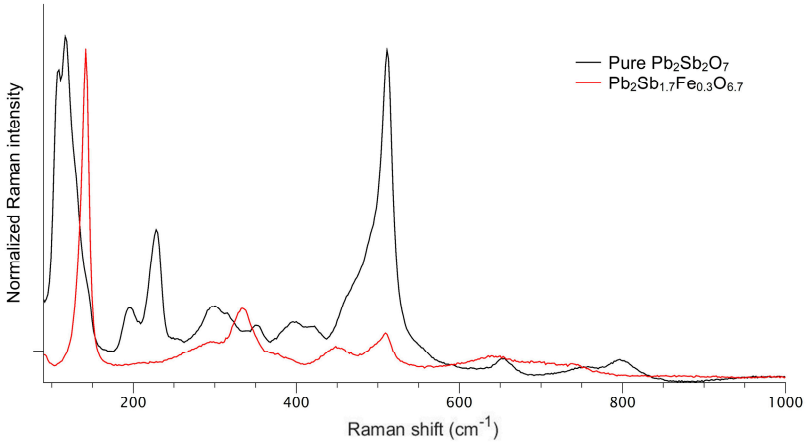


Figure 17. Raman spectra of lead antimonates synthesized for this study: pure $Pb_2Sb_2O_7$ in black and Fe-substituted $Pb_2Sb_{1.7}Fe_{0.3}O_{6.7}$ in red. The spectra have been normalized to the intensity of the peak at 140 cm^{-1}. These spectra are useful as references to interpret the Raman spectra of lead antimonates in the glazes shown in Figure 16.

The Raman spectrum of the pure $Pb_2Sb_2O_7$ of this study, in black in Figure 17, is characterized by two equivalently intense features: a peak at 513 cm^{-1} and a double peak at 107 cm^{-1} and 117 cm^{-1}. Other well-defined features are two peaks at 198 cm^{-1} and 226 cm^{-1}, then low-intensity peaks at 300 cm^{-1}, 350 cm^{-1}, 400 cm^{-1}, and 423 cm^{-1}. The intense peak at 513 cm^{-1} bears a low-frequency shoulder at 475 cm^{-1}. In the Fe-substituted $Pb_2Sb_{1.7}Fe_{0.3}O_{6.7}$ compound, the intensity of the 513 cm^{-1} peak has considerably decreased with respect to the low-frequency intense peak, which has shifted to 140 cm^{-1} and has become unique (no doublet). The 200–480 cm^{-1} range has been globally modified and contains a large main peak at 338 cm^{-1}, with shoulders at 305 and 393 cm^{-1}, and another large, low-intensity peak at 455 cm^{-1}. Rosi et al. have published an analysis of the Raman spectra of $Pb_2Sb_2O_7$ as pure form with different Pb/Sb ratio and of $Pb_2Sb_2O_7$ with Sn and Zn substitution for Sb [27]. The spectrum of our $Pb_2Sb_2O_7$ synthesized reference is very similar to their spectra for pure $Pb_2Sb_2O_7$. In particular, the peak at 513 cm^{-1}, which is attributed to the symmetric stretching of SbO_6 octahedra, tends to be more intense than the double peak at 107–120 cm^{-1}, attributed to the stretching of the Pb_4O tetrahedron. Substituting Sb^{5+} by Zn^{2+} yields spectra very similar to the spectrum of our $Pb_2Sb_{1.7}Fe_{0.3}O_{6.7}$ reference, with the collapse of the 513 cm^{-1} peak, probably due to the disruption of the SbO_6 network, and the high-frequency shift of the 107–120 cm^{-1} peak towards 140 cm^{-1}. This similarity of the Raman spectra of Pb-Sb-Zn and Pb-Sb-Fe antimonates has also been emphasized in the study of Cartechini et al. [39].

The Raman spectra of the lead antimonates in the orange–yellow glazes of Khorsabad, Aššur, and Babylon all correspond to the modified pyrochlore structure bearing Fe^{3+}, and their grouping per colour puts in evidence common spectral alterations according to the colour. Among the three types of lead antimonates, the Raman spectra of the dark yellow (DY) are very close to the spectrum of the $Pb_2Sb_{1.7}Fe_{0.3}O_{6.7}$ reference. This is consistent with the composition of the DY antimonate that is enriched in Fe substituting Sb, with 0.32 to 0.37 of Fe per formula unit. In comparison with this now well-identified spectrum, the two other spectra, for pale yellow and orange–red colours, show characteristic differences. For the PY of Khorsabad and Aššur, the 513 cm^{-1} peak has a higher intensity with respect to the peak at 140 cm^{-1}, and this latter peak is divided into two peaks at about 127 and 140 cm^{-1}. Moreover, the intensities of the small peaks at 206 and 393 cm^{-1} are slightly higher. According to the EDX results, these spectral modifications can be associated with the enrichment of Ca substituting Pb in the pyrochlore structure. In the BSE image of zone (1) in Figure 10, the white to grey contrast corresponds to a range of enrichment in Ca. By carrying out a Raman mapping of this zone, we have noticed that the more Ca in the pyrochlore, the more intense the 127 cm^{-1} contributions to the first peak (Raman

and EDX mapping of zone 1, not shown). Note that for Babylon, as described before, PY antimonates appeared much less numerous than the O–R and DY ones in the yellow glazes from Babylon, and it was difficult to distinguish them optically. Therefore, a series of Raman spectra for DY/PY crystals are presented together (bottom of Figure 16b). These spectra remarkably show the same intensity variations as for Khorsabad DY/PY: when the intensity of the 513 cm^{-1} peak is high, that of the 127 cm^{-1} shoulders and 393 cm^{-1} peak are also high (the tendency is less clear for the 206 cm^{-1} peak). For Aššur, the two spectra for DY and PY could be distinctly obtained, as shown in Figure 16c.

On the other hand, the Raman spectrum of the O–R colour bears similar modifications as the PY colour mentioned for Khorsabad and Aššur (more intense 513 cm^{-1} peak and the 140 cm^{-1} peak becomes a doublet); however, the 206 and 393 cm^{-1} peaks are generally weak, and the most characteristic feature is a wide peak at about 615–630 cm^{-1}. This type of lead antimonate is particularly enriched in iron, leading us to the suggestion that this feature may be a signature of some Fe-oxide-rich surrounding of the antimonate. A more detailed two-dimensional analysis with high spatial resolution, such as μ-XRF [24], would be necessary to answer. In these O–R spectra, the double peak at 127–140 cm^{-1} and the intensity of the 206 cm^{-1} peaks are variable, which may be consistent with the variability of Ca content observed by EDX. The same O–R spectrum with the 630 cm^{-1} band has been encountered in all the Italian Renaissance Majoliques plates and tiles of the study of Rosi et al. [28]. Among the various pigments used by these authors as internal references, this spectrum is close, but not identical, to the spectrum of the pigment PV-NY-34 synthesized with Pb_3O_4 and Sb_2O_3 and Pb:Sb = 3:2, without any flux. This pigment was heterogeneous, and its XRD pattern could not be clearly attributed to any Pb-Sb compound of the PDF database. In our case, the stoichiometry of this phase as obtained by EDX is close to that of the pyrochlore, and an association with an excess of Fe is certain.

Raman spectra of the other antimonate compounds found in the orange glazes of Khorsabad are depicted in Figure 18. In Figure 18a, the red spectrum has been measured on the big isotropic calcium antimonate crystals of the "bunch of grapes" group in zone (2) of Figure 10. The blue spectrum has been taken on needle-shaped Ca-antimonate crystals as such present at the bottom of the bunch of grapes in zone (2) or in the middle of the Pb-antimonate circle in zone (3) of Figure 10. Both spectra relate to the same $CaSb_2O_6$ phase, characterized by the sharp peak at 671 cm^{-1}. At last, Figure 18b shows various spectra obtained for Fe-antimonate crystals in two different bricks. Fe-antimonates are not abundant in these glazes, and we did not study them closely. For the one group examined by SEM-EDX, the contrast on BSE images was homogeneous, and the Fe:Sb EDX ratio was very close to 1:1. However, the Raman spectra are diverse, with different positions for the most intense peaks, so there must be some chemical and structural heterogeneity within this composition.

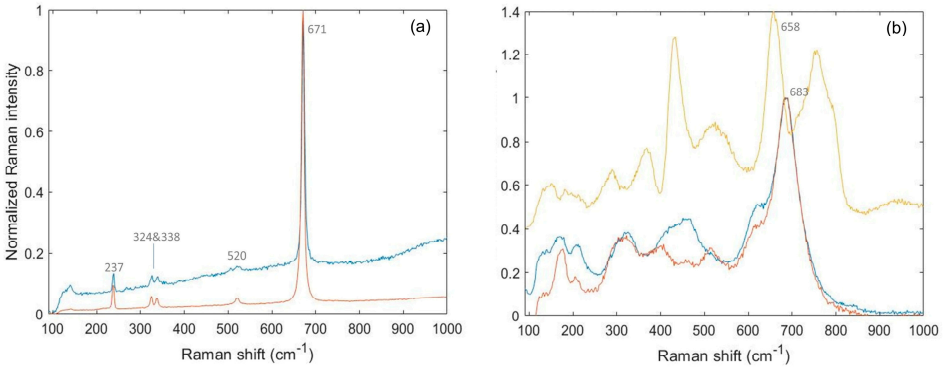


Figure 18. (**a**) Raman spectra of calcium antimonates with needle-like microstructure (blue) and with cubic-shaped microstructure (red) taken from the K-N8080 brick in the area of Figure 8b also referred to as zone 2 in Figure 10. (**b**) Raman spectra of the iron antimonates taken from brick K-AO29710 (yellow spectrum) and brick K-N8123 (red and blue spectra).

3.3. The Glass Matrix of the Black and Orange–Yellow-Coloured Glazes

The type of glass matrixes used for the black and the orange–yellow colours have been determined through the EDX analysis of their composition in homogeneous areas far away from the inclusions. Because the glass phase has totally disappeared in the Aššur glazes (from SEM observations of polished cross-sections, the glazes appear over their entire thickness as a mass of reprecipitated material containing various inclusions), only Khorsabad and Babylon are considered in this paragraph. Table 5 reports the average composition of the glass phase in every investigated sample. From this, an average composition of the glass phase for every colour and corpus has been computed and given in bold to allow for comparison. In the case of Babylon black glazes, we have differentiated the blacks used to draw lines (contour lines or patterns) from the black used for flat decor (only one example B-VA17275) because the difference in composition was significant. For Khorsabad, the compositions for lines and decors were not so distinct, and only one mean composition has been computed.

Table 5. Average EDX analyses (oxide wt.%) of the glass matrix in the black and orange–yellow (o/y) samples of Khorsabad and Babylon investigated in this study (standard deviation in grey). The analyses have been carried out far away from the crystals or from the copper sulphide nanoparticles. loq: limit of quantification. * These Pb, Sb and Cu contents are very likely due to a running with the adjacent glaze (orange, yellow, white, turquoise or green) during firing. ** This loq is higher due to the presence of Pb in the glaze matrix (overlapping of PbM and SK_α lines).

Glaze	Sample		SiO_2	Na_2O	MgO	K_2O	CaO	Al_2O_3	Cl	Fe_2O_3	PbO	Sb_2O_3	CuO	SO_3
BLACK Khorsabad	K-N8098 (decor)	Mean	68.98	17.00	2.83	2.93	5.63	1.18	0.44	0.34	<loq	<loq	0.07	0.60
		Sigma	0.65	0.30	0.17	0.05	0.09	0.21	0.11	0.04			0.04	0.13
	K-N8080 (decor)	Mean	70.83	14.34	2.64	3.81	5.46	1.22	0.39	0.31	<loq	0.16	0.09	0.74
		Sigma	0.79	0.29	0.16	0.05	0.35	0.14	0.11	0.09		0.11	0.06	0.24
	K-N8099 (line)	Mean	68.87	12.35	2.63	4.19	6.33	1.9	0.73	0.75	<loq	1.01	0.28	0.92
		Sigma	1.61	2.17	0.08	0.02	0.23	0.37	0.15	0.13		0.08	0.03	0.13
	Mean black samples		69.56	14.56	2.70	3.64	5.81	1.43	0.52	0.47	<loq	0.39	0.15	0.75
BLACK Babylon	B-LPS (line)	Mean	71.82	10.84	3.43	3.96	4.06	1.61	0.43	1.05	2.35 *	0.9 *	<loq	<loq **
		Sigma	0.85	0.20	0.08	0.09	0.10	0.17	0.01	0.08	0.25	0.18		
	B-VA17274 (line)	Mean	72.34	10.83	3.56	3.81	4.88	1.81	0.37	1.19	<loq	0.15*	0.65*	0.36
		Sigma	1.02	0.08	0.18	0.06	0.32	0.17	0.04	0.05		0.15	0.06	0.02
	B-VA17282 (line)	Mean	74.30	11.64	3.35	3.19	3.57	1.49	0.43	1.13	<loq	0.31*	<loq	0.44
		Sigma	0.08	0.11	0.02	0.05	0.04	0.04	0.03	0.18		0.01		0.01
	B-VA17270 (line)	Mean	71.07	13.02	3.52	4.09	4.35	1.57	0.43	0.94	0.22	0.15*	0.22*	0.42
		Sigma	0.40	0.06	0.04	0.18	0.07	0.17	0.00	0.26	0.01	0.08	0.18	0.01
	Mean black samples (lines)		72.38	11.58	3.46	3.76	4.22	1.62	0.42	1.08	0.64*	0.38*	0.22*	0.31
	B-VA17275 (decor)	Mean	63.78	16.26	4.82	4.21	6.52	2.24	0.55	1.05	<loq	<loq	<loq	0.56
		Sigma	0.25	0.01	0.01	0.04	0.15	0.10	0.01	0.07				0.00
ORANGE Khorsabad	K-AO29710	Mean	68.46	10.72	0.96	1.87	2.63	1.03	0.66	5.16	6.94	1.58		
		Sigma	5.67	4.31	0.30	0.31	0.57	0.32	0.18	3.78	0.58	0.62		
	K-N8080	Mean	64.90	15.50	2.50	2.97	3.30	0.97	0.62	2.45	5.80	0.99		
		Sigma	0.23	0.16	0.09	0.03	0.23	0.10	0.15	0.51	0.27	0.16		
	K-N8098	Mean	67.95	13.55	2.67	3.04	3.62	0.92	0.74	1.80	4.88	0.85		
		Sigma	1.65	1.67	0.21	0.01	0.21	0.07	0.03	0.20	0.17	0.06		
	K-N8105	Mean	64.89	10.97	2.49	3.09	3.90	1.19	0.38	3.67	7.65	1.77		
		Sigma	1.81	0.73	0.17	0.04	0.30	0.13	0.12	0.55	0.71	0.45		
	K-N8123	Mean	66.32	14.66	2.58	3.48	3.67	0.98	0.87	2.22	4.32	0.89		
		Sigma	0.73	0.36	0.11	0.07	0.45	0.13	0.08	0.81	0.22	0.10		
	Mean orange samples		66.50	13.08	2.24	2.89	3.42	1.02	0.65	3.06	5.92	1.22		
	Mean orange samples with substraction of PbO and Sb_2O_3		71.61	14.09	2.41	3.11	3.68	1.10	0.70	3.30	0.00	0.00		
YELLOW Babylon	B-LPS	Mean	62.93	13.61	4.62	3.40	4.61	1.80	0.49	1.06	6.26	1.23		
		Sigma	0.52	0.21	0.09	0.05	0.10	0.08	0.02	0.01	0.68	0.29		
	B-VA17268	Mean	62.95	12.78	3.74	3.39	4.00	1.40	0.50	0.99	8.58	1.67		
		Sigma	1.41	0.10	0.08	0.12	0.05	0.12	0.06	0.44	0.53	0.31		
	Mean yellow samples		62.94	13.19	4.18	3.39	4.30	1.60	0.50	1.02	7.42	1.45		
	Mean yellow samples with substraction of PbO and Sb_2O_3		69.07	14.48	4.59	3.73	4.72	1.75	0.55	1.12	0.00	0.00		

The glazes are all highly sodic (about 14 wt.% Na_2O) with moderate lime composition (3.5–6.5 wt.% CaO) and they bear a significant amount of MgO and K_2O which classifies them as High Magnesium glasses (HM) according to the widely used criterion that the proportion of each of these two oxides is greater than 1.5 wt.% [40–42]. This indicates a plant ash origin for the fluxes, as expected for Iron Age glazes from the Near East [14]. The Na_2O/K_2O, Na_2O/CaO and Na_2O/MgO weight ratio are calculated in Table 6 along with the range of ratio published in Ref. [2] for similar glazes stemming from Nimrud (Neo-Assyrian Period) and Babylon (Neo-Babylonian Period).

Table 6. Weight ratio of flux oxides in the glass phase of Khorsabad and Babylon glazes of this study, compared with similar Mesopotamian glasses in the literature (in italics—from a total of 35 analyses of Near East glazes from 1400 BC to 600 AD reviewed in Ref. [2]). Numbers in bold denote values outside the range reported in Ref. [2].

Glaze	Na_2O/K_2O	Na_2O/CaO	Na_2O/MgO
Khorsabad black	4.0	2.5	5.4
Khorsabad orange	4.5	**3.8**	**5.8**
Babylon black (lines)	3.1	2.7	3.3
Babylon black (flat décor)	3.9	2.5	3.4
Babylon yellow	3.9	3.1	3.2
Nimrud (plaque, various, Neo-Assyrian)	*2.0–4.7*	*2.0–2.5*	*3.1–5.3*
Babylon (brick, Neo-Babylonian)	*3.6–4.6*	*2.2–3.1*	*3.6–5.2*

This comparison in Table 6 indicates a very good correspondence of these glazes with other glazes of the region and similar period, validating the consistencies of these analyses and the same glass-making technique with the same type of flux in this area and period. More largely, a close examination of Tables 5 and 6 shows that there is no significant difference between the glass composition in Khorsabad glaze and in Babylon glaze (other than the black glaze of brick B-VA17275 described hereafter).

Regarding the black colour, for Khorsabad, similar glass matrix compositions were found whether the glaze was used for contour line purposes or as flat decoration. For Babylon instead, the flat black glaze (brick B-VA17275) is richer in flux elements (alkalis and alkaline earths) and significantly poorer in silica (SiO_2 near 64 wt.%) compared to the black lines (SiO_2 greater than 71 wt.%). The latter is closer to the compositions found for Khorsabad. Note that numerous inclusions identified as quartz (by μ-Raman) were observed in the black lines (Figure 6e), except for the black glaze of brick fragment B-VA17274. Possibly quartz grains, not finely grounded, have been added to the glassy batch as an "inglaze", possibly to increase the refractarity and viscosity of the contour line during the firing. We emphasize that the analyses of the glass matrixes were carried out far away from these quartz grains. It is possible, however, that the analytical results contain a small contribution from quartz-like inclusions that are found deeper in the glaze and, therefore, not visible from the surface. This could explain the slightly higher silica content found in these Babylon black lines compared to Khorsabad black.

The glass matrixes of the orange–yellow glazes contain PbO and Sb_2O_3 oxides (or Sb_2O_5, as the redox state is unknown from these analyses) in addition to the main glass oxides. The high standard deviations measured for these oxides (Table 5) suggest that their presence is due to the antimonate pigments and not to an intentional addition in the glass composition. Indeed, when subtracting the PbO and Sb_2O_3 content from the glass composition, all the other oxide contents become similar to the glass matrix of the black colour for both corpora (excepting the B-VA17275 black decor)

Moreover, the mean PbO/Sb_2O_3 weight ratio measured in the glass matrix is 4.2 (Khorsabad) and 5.1 (Babylon). The lead antimonate crystals measured in this study have PbO/Sb_2O_3 weight ratio of 1.7 to 1.9. The excess in PbO may pre-exist in the pigment and be dissolved in the glass, as already stated by other authors [29,43]. The excess lead would indeed facilitate the initial formation of lead antimonate during its ex situ prepara-

tion [43]. Another possibility is that the added lead antimonates have partially dissolved in the glass during firing, and PbO would stay incorporated in the glass, while the less soluble Sb_2O_3 would precipitate as another phase(s). It is interesting to notice that due to the additional presence of PbO in the glass matrix, the orange–yellow glazes have a lower melting point than the black lines. This is also the case of the black glaze used as flat decor on brick B-VA17275 that shows a lower SiO_2 content and a higher amount of flux elements (alkali and alkali earth oxides). It is possible that the use of black lines with a higher melting point and viscosity was of technological interest to prevent other glazes from running together during firing, as already argued for glazes from Susa [6].

The Fe_2O_3 content is very interesting to look at. It is very low, below 1.2 wt.%, in the black colour of both corpora and in the yellow colour of Babylon, while it is significantly higher in the orange colour of Khorsabad (about 3.3 wt.%). Moreover, the standard deviations measured for the Fe_2O_3 content are also quite high in the orange–yellow glass matrix. This indicates that the Fe_2O_3 has been added with the lead antimonate, either intentionally and separately (Fe_2O_3 hematite was added in the mixture with lead antimonates and glass components) or unintentionally due to the lead antimonate preparation that may have included iron-bearing raw materials. The observation of well-defined hematite particles in the orange–yellow glazes supports the first hypothesis. As already stated, our low magnification microscopic observations also tend to indicate that there are more hematite particles in Khorsabad orange than in Babylon yellow. Thus, we think that at least a part of the Fe_2O_3 has been added separately, together with lead antimonate pigments, in the same type of glass frit as used for the black colour.

At last, it is interesting to notice that the CaO content is systematically lower in the Khorsabad orange glazes compared with the Khorsabad black glazes. In this colour, the Na_2O/CaO ratio even exceeds the range of ratios reported for Nimrud and Babylon (Table 6). This decrease in CaO content is likely related to the precipitation of Ca-antimonate crystals resulting from the instability of the lead antimonate in the glaze and to the incorporation of Ca in the lead-antimonate as described before and shown in Figure 10.

4. Discussion

Several authors describe black vitreous materials, mainly dated to the 1st millennium BC, in which the content of Mn and Fe oxides are obviously too low to give a deep black hue: in the black glazes of some Sassanid vases, in some black glazes of the Ishtar Gate bricks [44,45], but no explanation is proposed. In this study, an unusual practice for colouring black glazes was highlighted. This technique is not based on the use of colouring oxide but on the presence of Cu,(Pb),(Sb),(Fe) sulphide nanoparticles within the glaze. These sub-micrometric particles were observed for the corpus of Khorsabad and Babylon. In the literature, the presence of Cu, (Fe) sulphide nanoparticles are reported for two black glass beads from Nuzi (north of present-day Iraq) dated back to the mid-2nd millennium BC and for black glasses from Hasanlu (northwest of present-day Iran) dated back to the 9th century BC [12,46,47]. Strings of copper sulphide nanoparticles have also been put in evidence in a similar alkali glaze of Middle Islamic ceramics from Jerash in northern Jordan; this glaze is characterized by an intense dark blue hue, although its CuO content is low (<1 wt.%) [48]. The authors assume that they are responsible for the black colouration [12,47]. In an aqueous solution, apart from the mention of a black colouration given by Cu_xS particles, it is also reported that the presence of such particles can result in a dark green colouration [49–51]. The black glaze of brick fragment B-VA17275 contains less of these particles as compared to the other black glazes of Babylon, and the colour of this sample appears dark green—blackish in some areas. Considering that S and Fe are detected in the glass matrix at levels of about 0.6 wt.% (SO_3), and 1 wt.% (Fe_2O_3) (Table 5), the contribution of the chromophore Fe^{3+}-S^{2-} may be suspected, as Fe and S contents of less than 1000 ppm are sufficient to colour glass. This chromophore is likely to be present in all black glazes of this study, as demonstrated by the 375 cm^{-1} and 420 cm^{-1} contributions in their Raman spectra [36,37]. The presence of this chromophore implies reducing conditions

that can be controlled by the atmosphere, which prevails when the glass is melted and/or by various redox species within the melt. The black glazes have been fired together with the orange–yellow glazes on the same bricks, and the latter is obviously oxidized (presence of Fe_2O_3 hematite). Therefore, we suggest that reducing conditions have been achieved chemically in the black glazes, either with an external reducer (carbon-bearing material) or possibly by a copper-sulphide bearing raw material itself (as possibly Cu_2S covellite). In the latter hypothesis, the partial oxidation, dissolution, and recrystallization of this copper-sulphide bearing raw material in the glaze during the firing would have produced the nanoparticles, while it would have also consumed the oxygen in the surrounding glass matrix and generated the Fe^{3+}-S^{2-} chromophore. The black colour may then result from the addition of the copper sulphide particles and the matrix absorption contributions. Note that the distinctive band at 990 cm^{-1} in our spectra reveals that sulphur also exists in the +VI redox state in the glass matrix (Figure 7). The observation of both oxidation states of sulphur is unexpected, except if we suppose a chemical inhomogeneity of the glass matrix at the micrometre scale that is the scale of the Raman analysis.

Thus, as stated by Stapleton, the presence of copper sulphide nanoparticles would be a hint of the use of a copper sulphide ore [12,47]. Copper sulphide ores were commonly used in Mesopotamia from the late Bronze Age [52]. It is possible that the chemical variability of these nanoparticles, in particular the presence of the elements Pb, Sb or Fe, reflects the use of different ores. The raw materials, firing process, and the conditions of formation of these nanoparticles within the glass melt remain largely unclear, and replication experiments would be useful to progress on it.

Regarding the colouring technique for Aššur black glazes, this study showed a change between the 9th and the 8th century BC. The fact that these glazes are today very heavily weathered, without any relics of original vitreous material, was strongly limiting for this study. However, it appeared clearly that from the 8th century BC onwards, the craftsmen no longer used Mn oxide or any other colouring oxide to produce the black. This black of the Aššur bricks remains enigmatic. It is interesting to note that during the study of a black glaze of an Aššur vessel (VAM collection, Inv. No. VA Ass 4169), probably dating from the 8th century BC and not completely altered, we were able to observe nanoparticles rich in copper and sulphur, but only in the unaltered part (the altered part having become whitish). Thus, the use of copper sulphide nanoparticles for black glaze would have occurred in Aššur around the 8th century BC and it is possible that this technique was also used for the bricks. Finally, from archaeological evidence including that highlighted in this study, it appears that this technology has been used in the northern region of ancient Mesopotamia at least from the middle of the 2nd millennium BC for colouring black glass (Nuzi and Hasanlu) and would have been introduced in Aššur and Khorsabad around the 8th century BC for colouring black glazes, lasting at least until the Neo-Babylonian Empire.

The investigation of the orange–yellow glazes in terms of matrix composition and chemical, microstructural, and structural characterisation of the lead antimonates pigments allows making assumptions about the colouring process. Their distribution within the glazes suggests that they were prepared ex situ. Very interestingly, three shades of lead antimonates pigments were observed within the same orange–yellow glaze, identified as orange–red, dark-yellow, and pale yellow. The compositional and structural results have revealed that the proportion of iron, calcium, and sodium that enter the pyrochlore structure of the lead antimonates is the main difference between these different shades: the iron content increases, and the calcium and sodium content decreases in the darkest shades (from pale yellow to dark yellow, the case of orange–red being more complex and possibly polyphasic). The presence of iron in the lead antimonate lattice is a common feature in ancient Egyptian and Roman yellow glass [29]. It was argued that the origin of the iron present in the Egyptian and Roman pigments was probably the result of contamination by iron minerals (introduced, for instance, with the source of lead antimonates, from clay crucibles, or from iron tools). Some authors have reported a higher amount of iron in the darker shades and have suggested on the contrary that extra iron was deliberately

added for the production of the pigment [22,53–55]. The fact that we have observed (a) well-mastered colour(s) within the orange–yellow range for each corpus (one orange for Khorsabad, one yellow for Babylon and one orange, one yellow, and one pale yellow for Assur) and the presence of hematite in greater quantity in the orange glazes of Khorsabad compared to the yellow glazes of Babylon speaks for a deliberate addition of presumably hematite or any hematite precursor (as a refined red clay?) in controlled quantities for the Neo-Assyrian and Neo-Babylonian glazes.

At last, the chemical instability of the lead antimonate pigments under the firing conditions of these glazes has been put in evidence in this study. Such a chemical reactivity during the firing has been demonstrated in the literature, for instance, in maiolica decorations opacified by Naples yellow and cassiterite [28]. Here, modifications of the lead antimonate pyrochlore touch both the Sb site (Sb/Fe substitution) and the Pb site (Pb/Ca substitution). The latter substitution has not been described in the literature to the best of our knowledge. Examination of microstructures and chemical compositions of the lead antimonate crystals tend to indicate two processes: Pb^{2+}/Ca^{2+} interdiffusion within the crystals or their partial dissolution followed by $CaSb_2O_6$ precipitation [24].

5. Conclusions

The in-depth study by optical microscopy, SEM-EDX, and μ-Raman of glaze samples belonging to Aššur (9th to 7th BC), Khorsabad (8th century BC), and Babylon (6th BC) architectural glazed bricks have brought to light some very interesting features of the respective colouring agents of the orange–yellow and black glazes. For both Khorsabad and Babylon, the black glaze is coloured by copper sulphide nanoparticles distributed throughout the glaze, with a probable contribution of the Fe^{3+}-S^{2-} chromophore that has been detected by Raman. Although the black glazes of Aššur are heavily weathered, it was possible to state that the glazes dated back to the 9th century BC were coloured by Mn oxides, while later glazes (from 8th century BC onwards) did not show any trace of Mn oxides and may have been coloured using the same technique as revealed in Babylon and Khorsabad. Considering the composition of the glass matrix and the coexistence of black with other colours, we suggest that this technique may have consisted in employing copper sulphide ores, which may have provided the sulphur and the reducing conditions in the glass matrix. An additional reducing component may have also been necessary to stabilize the S^{2-} state. Experiments with replicates are necessary to study these hypotheses. From the sparse reports in the literature, this technique of black colouration has appeared as early as the mid-2nd millennium BC in Mesopotamia, and this study seems to indicate that it has been widely employed in the 8th to 6th century BC in the Neo-Assyrian and Neo-Babylonian Periods.

The macroscopic examination of the orange–yellow glazes reveals several well-mastered hues of this colour according to the corpus: a more orange hue for Khorsabad, a more yellow hue for Babylon, and at least three hues for Aššur: an orange, a yellow, and a pale greenish-yellow. This colour arises from the use of lead antimonate pigments, as usually observed in the Antiquity. The orange hue for Khorsabad is probably related to the additional presence of hematite in larger amounts than for Babylon. The microscopic-scale examination revealed the chemical complexity of the lead antimonates, with different ranges of chemical substitution, mainly Fe^{3+} in the Sb^{5+} site and Ca^{2+} in the Pb^{2+} site, related to different shades. The Ca^{2+}/Pb^{2+} substitution has not been described in the literature to the best of our knowledge. From microstructural evidence, it results from the chemical instability of the lead antimonate in the alkali lime melt. Its experimental study in the future should provide detailed information about the firing process. New perspectives are thus opened to gain deeper insight into the techniques of production of these impressive architectural decors and the transfer of know-how between the different periods and capitals in Mesopotamia.

Supplementary Materials: The following are available online at https://www.mdpi.com/article/10.3390/min12030311/s1 including Figure S1: XRF Cartography of the K-N8123 brick from Khorsabad, Figure S2: XRF Cartography of a glazed area of the A-810791 brick from Aššur, Figure S3: XRF Cartography of a glazed area of the A-810373 brick from Aššur; Figure S4: Final Rietveld plot for the 0.8 Fe sample, Table S1: Colour palette and colouring agents identified for the three different corpuses of glazed bricks: Khorsabad, Aššur and Babylon as given by visual examination and XRF analyses.

Author Contributions: Conceptualization, F.A., O.M. and A.B.; methodology, F.A., O.M., F.G. and A.B.; validation, all authors.; formal analysis and investigation, F.A., O.M., F.G., C.D. and G.W.; writing—original draft preparation, F.A., O.M. and A.B.; writing—review and editing, all authors; project administration and funding acquisition, H.G., A.F., A.B. and A.T. All authors have read and agreed to the published version of the manuscript.

Funding: This research was funded by the Deutsche Forschungsgemeinschaft (DFG) (study of the Aššur and Babylon bricks) and by the Fondation des Sciences du Patrimoine (FSP) (study of the Khorsabad bricks).

Data Availability Statement: Data is contained within the article or supplementary material. Further data can be made available on qualified request from the corresponding author.

Acknowledgments: The authors gratefully thank Sonja Radujkovic from the VAM for her help with the sampling of the Aššur and Babylon bricks and the photo-documentation. May-Sarah Zessin from the VAM is thanked for her assistance in conducting the XRF measurements in Berlin and for the data handling of the Aššur bricks. Thomas Calligaro from the C2RMF is thanked for the acquisition of XRF data on Khorsabad bricks. Stefan Kirstein from the Humboldt University (Berlin) is also acknowledged for having made available the Raman spectrometer Horiba X-Plora that contributed to the study of the glazes from Babylon and from Aššur. Stefan Simon and Stefan Röhrs from the Rathgen-Forschungslabor and Patrice Lehuedé and Marie-Hélène Chopinet are thanked for their support and fruitful discussions.

Conflicts of Interest: The authors declare no conflict of interest. The funders had no role in the design of the study; in the collection, analyses, or interpretation of data; in the writing of the manuscript, or in the decision to publish the results.

References

1. Fügert, A.; Gries, H. Chapter 1: 'I had baked bricks glazed in lapis lazuli color'—A brief history of glazed bricks in the Ancient Near East. In *Glazed Brick Decoration in the Ancient Near East, Proceedings of a Workshop at the 11th International Congress of the Archaeology of the Ancient Near East (Munich) in April 2018, Munich, Germany, 3–7 April 2018*; Fügert, A., Gries, H., Eds.; Archaeopress Publishing Ltd.: Oxford, UK, 2020; pp. 1–15.
2. McCarthy, B.; Paynter, S. Chapter 9: Production of glazed pottery and brickwork in the Near East. In *Production Technology of Faience and Related Early Vitreous Materials*; Tite, M.S., Shortland, A.J., Eds.; Oxford University School of Archaeology: Oxford, UK, 2008; pp. 187–198.
3. Paynter, S.; Tite, M.S. The evolution of glazing technologies in the Ancient Near East and Egypt. In *The Social Context of Technological Change. Egypt and the Near East, 1650–1550 BC*; Shortland, A.J., Ed.; Oxbow Books: Oxford, UK, 2001; pp. 239–254.
4. Gries, H.; Schmidt, K. The core-formed glass vessels from Middle Assyrian Aššur. *Z. Assyriol. Vorderasiat. Archäologie* **2020**, *110*, 242–275. [CrossRef]
5. Freestone, I. Technical examination of Neo-Assyrian glazed wall plaques. *Iraq* **1991**, *53*, 55–58. [CrossRef]
6. Holakooei, P. A multi-spectroscopic approach to the characterization of early glaze opacifiers: Studies on an Achaemenid glazed brick found at Susa, south-western Iran (mid-first millennium BC). *Spectrochim. Acta A Mol. Biomol. Spectrosc.* **2013**, *116*, 49–56. [CrossRef]
7. Holakooei, P.; Ahmadi, M.; Volpe, L.; Vaccaro, C. Early opacifiers in the glaze industry of first millenium BC Persia: Persepolis and Tepe Rabat. *Archaeometry* **2017**, *59*, 239–254. [CrossRef]
8. Holakooei, P.; Soldi, S.; De Lapérouse, J.F.; Caro, F. Glaze composition of the Iron Age glazed ceramics from Nimrud, Hasanlu and Borsippa. *J. Archaeol. Sci. Rep.* **2017**, *16*, 224–232.
9. Hedges, R. Pre-Islamic glazes in Mesopotamia-Nippur. *Archaeometry* **1976**, *18*, 209–238. [CrossRef]
10. Hedges, R.; Moorey, P. Pre-Islamic ceramic glazes at Kish and Nineveh in Iraq. *Archaeometry* **1975**, *17*, 25–43. [CrossRef]
11. Tite, M.S.; Shortland, A.J. Report on the scientific examination of a glazed brick from Susa: Glazes. In *Persiens Antike Pracht-Band 2*; Stöllner, T., Slotta, R., Vatandoust, A., Eds.; University of Pennsylvania Press: Philadelphia, PA, USA, 2004; pp. 338–390.
12. Stapleton, C. Glass and glaze analysis and technology from Hasanlu, period IVB. In *Peoples and Crafts in Period IVB at Hasanlu, Iran*; De Schauensee, M., Ed.; University of Pennsylvania Press: Philadelphia, PA, USA, 2011; pp. 87–102.

13. Bouquillon, A.; Kaczmarczyk, A.; Vandiver, P. Chapter 5: Faience production in the Near East and the Indus Valley. In *Production Technology of Faience and Related Early Vitreous Materials*; Tite, M.S., Shortland, A.J., Eds.; Oxford University School of Archaeology: Oxford, UK, 2008; pp. 93–109.
14. Holakooei, P. Chapter 2: Scientific research on the Iron Age glazes from Iran and Iraq: Past and future. In *Glazed Brick Decoration in the Ancient Near East, Proceedings of a Workshop at the 11th International Congress of the Archaeology of the Ancient Near East (Munich) in April 2018, Munich, Germany, 3–7 April 2018*; Fügert, A., Gries, H., Eds.; Archaeopress Publishing Ltd.: Oxford, UK, 2020; pp. 16–27.
15. Fügert, A.; Gries, H. Chapter 3: The reconstruction of the glazed brick facades from Ashur in the Vorderasiatisches Museum, Berlin (GlAssur Project). In *Glazed Brick Decoration in the Ancient Near East, Proceedings of a Workshop at the 11th International Congress of the Archaeology of the Ancient Near East (Munich) in April 2018, Munich, Germany, 3–7 April 2018*; Fügert, A., Gries, H., Eds.; Archaeopress Publishing Ltd.: Oxford, UK, 2020; pp. 28–46.
16. Gries, H.; Fügert, A. Neues Altes aus Assur-Das GlAssur-Projekt-Die Rekonstruktion der Glasurziegelfassaden aus Assur im Vorderasiatischem Museum. *Alter Orient Aktuell* **2019**, *16*, 11–17.
17. Gries, H.; Fügert, A. The glazed brick façades from Ashur in the Vorderasiatisches Museum Berlin in context of the North-Western Iranian glazed bricks. In *Proceedings of Iron Age in Western Iran and the Neighboring Regions: Problems and Priorities*; Hassanzadeh, Y., Vahdati, A.A., Karimi, Z., Eds.; Research Institute of Cultural Heritage and Tourism: Tehran, Iran; National Museum of Iran: Tehran, Iran; Kurdistan Province ICHHTO: Sanandaj, Iran, 2019; pp. 258–272.
18. Thomas, A. Chapter 4: Glazed bricks by the dozens: A Khorsabad jigsaw reassembled at the Louvre. In *Glazed Brick Decoration in the Ancient Near East, Proceedings of a Workshop at the 11th International Congress of the Archaeology of the Ancient Near East (Munich) in April 2018, Munich, Germany, 3–7 April 2018*; Fügert, A., Gries, H., Eds.; Archaeopress Publishing Ltd.: Oxford, UK, 2020; pp. 48–84.
19. Thomas, A. Un puzzle en briques émaillées de Khorsabad. *Rev. Assyriol. Archeol. Orient.* **2020**, *114*, 103–158. [CrossRef]
20. Pedersén, O. Chapter 6: The glazed bricks that ornamented Babylon—A short overview. In *Glazed Brick Decoration in the Ancient Near East, Proceedings of a Workshop at the 11th International Congress of the Archaeology of the Ancient Near East (Munich) in April 2018, Munich, Germany, 3–7 April 2018*; Fügert, A., Gries, H., Eds.; Archaeopress Publishing Ltd.: Oxford, UK, 2020; pp. 96–122.
21. Schmidt, K. *Glass and Glass Production in the Near East during the Iron Age. Evidence from Objects, Texts and Chemical Analysis*; Archaeopress Publishing Ltd.: Oxford, UK, 2019.
22. Kaczmarczyk, A. Méthodes d'analyse. Caractérisations des compositions en fonction des époques et des régions—Historical and regional variations in compositions. In *Faïences et Matières Vitreuses de l'Orient Ancien*; Bouquillon, A., Caubet, A., Kaczmarczyk, A., Matoían, V., Eds.; Snoeck–Musée du Louvre: Ghent, Belgium; Paris, France, 2007; pp. 17–27.
23. Kaczmarczyk, A.; Hedges, R. Chap. 2—The elemental composition of faience glazes. In *Ancient Egyptian Faience—An Analytical Survey of Egyptian Faience from Predynastic to Roman Times*; Kaczmarczyk, A., Hedges, R., Eds.; Aris & Phillips Ltd.: Warminster, UK, 1983; pp. 20–139.
24. Lahlil, S.; Cotte, M.; Biron, I.; Szlachetko, J.; Menguy, N.; Susini, J. Synthesizing lead antimonate in ancient and modern opaque glass. *J. Anal. At. Spectrom.* **2011**, *26*, 1040–1050. [CrossRef]
25. Salinas, E.; Pradella, T.; Matin, M.; Tite, M. From tin- to antimony-based yellow opacifiers in the early Islamic Egyptian glazes: Regional influences and ruling dynasties. *J. Archaeol. Sci. Rep.* **2019**, *26*, 101923. [CrossRef]
26. Caubet, A.; Pierrat-Bonnefois, G. *Catalogue d'exposition: Faïences de l'Antiquité. De l'Égypte à l'Iran*; Musée du Louvre: Paris, France, 2005.
27. Rosi, F.; Manuali, V.; Miliani, C.; Brunetti, B.G.; Sgamellotti, A.; Grygar, T.; Hradil, D. Raman scattering features of lead pyroantimonate compounds: Part I: XRD and Raman characterization of $Pb_2Sb_2O_7$ doped with tin and zinc. *J. Raman Spectrosc.* **2009**, *40*, 107–111. [CrossRef]
28. Rosi, F.; Manuali, V.; Grygar, T.; Bezdicka, P.; Brunetti, B.G.; Sgamellotti, A.; Burgio, L.; Seccaroni, C.; Miliani, C. Raman scattering features of lead pyroantimonate compounds: Implication for the non-invasive identification of yellow pigments on ancient ceramics. Part II. In situ characterisation of Renaissance plates by portable micro-Raman and XRF studies. *J Raman Spectrosc.* **2011**, *42*, 407–414. [CrossRef]
29. Molina, G.; Odin, G.; Pradell, T.; Shortland, A.J.; Tite, M.S. Production technology and replication of lead antimonate yellow glass from New Kingdom Egypt and the Roman Empire. *J. Archaeol. Sci.* **2014**, *41*, 171–184. [CrossRef]
30. Holakooei, P. A technological study of the elamite polychrome glazed bricks at Susa, south-western Iran. *Archaeometry* **2014**, *56*, 764–783. [CrossRef]
31. Caubet, A.; Kaczmarczyk, A. Les briques glaçurées du palais de Darius: La frise des archers. *Techné* **1998**, *7*, 23–26.
32. Jung, M.; Hauptmann, A. Katalog der Ausstellung des Deutschen Bergbau-Museums Bochum, Band 2. In *Persiens Antike Pracht: Bergbau, Handwerk, Archäologie*; Stöllner, T., Slotta, R., Vatandoust, A., Eds.; Deutschen Bergbau-Museums Bochum: Bochum, Germany, 2004; pp. 390–392.
33. Schlick-Nolte, B.; Werthmann, R. Glass vessels from the burial of Nesikhons. *J. Glass Stud.* **2003**, *45*, 11–34.
34. Schreurs, J.; Brill, R. Iron and sulfur related colors in ancient glasses. *Archaeometry* **1984**, *26*, 199–209. [CrossRef]
35. Hradil, D.; Grygar, T.; Hradilova, J.; Bezdicka, P.; Grunwaldova, V.; Fogas, I.; Miliani, C. Microanalytical identification of Pb-Sb-Sn yellow pigment in historical European paintings and its differentiation from lead tin and Naples yellows. *J. Cult. Herit.* **2007**, *8*, 377–386. [CrossRef]

36. Ceglia, A.; Nuyts, G.; Cagno, S.; Meulebroeck, W.; Baert, K.; Cosyns, P.; Nys, K.; Thienpont, H.; Janssens, K.; Terryn, H. A XANES study of chromophores: The case of black glass. *Anal. Methods* **2014**, *6*, 2662–2671. [CrossRef]
37. Prinsloo, L.; Colomban, P. A Raman spectroscopic study of the Mapungubwe oblates: Glass trade beads excavated at an Iron Age archaeological site in South Africa. *J. Raman Spectrosc.* **2008**, *39*, 79–90. [CrossRef]
38. Lenoir, M.; Grandjean, A.; Poissonet, S.; Neuville, D. Quantitation of sulfate solubility in borosilicate glasses using Raman spectroscopy. *J. Non-Cryst. Solids* **2009**, *355*, 1468–1473. [CrossRef]
39. Cartechini, L.; Rosi, F.; Miliani, C.; D'Acapito, F.; Brunetti, B.; Sgamellotti, A. Modified Naples yellow in Renaissance majolica: Study of Pb-Sb-Zn and Pb-Sb-Fe ternary pyroantimonates by X-ray absorption spectroscopy. *J. Anal. At. Spectrom.* **2011**, *26*, 2500–2507. [CrossRef]
40. Sayre, E.; Smith, R. Compositional categories of ancient glass. *Science* **1961**, *133*, 1824–1826. [CrossRef] [PubMed]
41. Henderson, J. The early materials of early glass production. *Oxf. J. Archeol.* **1985**, *4*, 267–291. [CrossRef]
42. Freestone, I. Glass production in Late Antiquity and the Early Islamic period: A geochemical perspective. *Geol. Soc. Spec. Publ.* **2006**, *257*, 201–216. [CrossRef]
43. Shortland, A.J. The use and origin of antimonate colorants in early egyptian glass. *Archaeometry* **2002**, *44*, 517–530. [CrossRef]
44. Bouquillon, A.; Caubet, A.; Kaczmarczyk, A.; Matoían, V. *Faïences et Matières Vitreuses de l'Orient Ancien*; Bouquillon, A., Caubet, A., Kaczmarczyk, A., Matoían, V., Eds.; Snoeck–Musée du Louvre: Ghent, Belgium; Paris, France, 2007.
45. Fitz, S. Die Farbglasuren spätbabylonischer Wandverkleidungen—The colored glazes of Neo-Babylonian wall facings. *Ceram. Forum Int. Ber. Der Dtsch. Keram. Ges.* **1982**, *59*, 179–185.
46. Kirk, S. The Vitreous Materials from the 2nd Millennium BC City of Nuzi: Their Preservation, Technology and Distribution. Ph.D. Thesis, Cranfield University, Cranfield, UK, 2009.
47. Stapleton, C.; Swanson, S. Batch material processing and glassmaking technology of 9th century B.C. Artifacts excavated from the site of Hasanlu, northwest Iran. *Mat. Res. Soc. Symp. Proc.* **2002**, *712*, II7.4.1–II7.4.7. [CrossRef]
48. Ting, C.; Lichtenberger, A.; Raja, R. The technology and production of glazed ceramics from Middle Islamic Jerash, Jordan. *Archaeometry* **2019**, *61*, 1296–1312. [CrossRef]
49. Arshad, M.; Wang, Z.; Nasir, J.A.; Amador, E.; Jin, M.; Li, H.; Chen, Z.; Rehman, Z.; Chen, W. Single source precursor synthesized CuS nanoparticles for NIR phototherapy of cancer and photodegradation of organic carcinogen. *J. Photochem. Photobiol. B* **2020**, *214*, 112084. [CrossRef]
50. Coughlan, C.; Ibanez, M.; Dobrozhan, O.; Singh, A.; Cabot, A.; Ryan, K.M. Compound copper chalcogenide nanocrystals. *Chem. Rev.* **2017**, *117*, 5865–6109. [CrossRef]
51. Gargioni, C.; Borzenkov, M.; D'Alfonso, L.; Sperandeo, P.; Polissi, A.; Cucca, L.; Dacarro, G.; Grisoli, P.; Pallavicini, P.; D'Agostino, A.; et al. Self-assembled monolayers of copper sulfide nanoparticles on glass as antibacterial coatings. *Nanomaterials* **2020**, *10*, 352. [CrossRef]
52. De Ryck, I.; Adriaens, A.; Adams, F. An overview of Mesopotamian bronze metallurgy during the 3rd millennium BC. *J. Cult. Herit.* **2005**, *6*, 261–268. [CrossRef]
53. Freestone, I.; Stapleton, C. Composition, technology, and production of coloured glasses from mosaic vessels of the Early Roman Empire. In *Glass of the Roman Empire*; Bayley, J., Freestone, I., Jackson, C., Eds.; Oxbow Books: Oxford, UK, 2015; pp. 61–76.
54. Verita, M.; Magetti, M.; Sagui, L.; Santopadre, P. Colors of Roman glass: An investigation of the yellow sectilia in the Gorga collection. *J. Glass Stud.* **2013**, *55*, 21–34.
55. Moretti, C.; Hreglich, S. Opacification and colouring of glass by the use of «anime». *Glass Technol.* **1984**, *25*, 277–282.